Biointerface Research in Applied Chemistry
Open-Access Journal (ISSN: 2069-5837)

Article
Volume 13, Issue 4, 2023, 365
https://doi.org/10.33263/BRIAC134.365

Structural, Characterization, Biological Activity, and DFT Studies on some Novel Ruthenium 2-Aminomethyl Benzimidazole Complexes

Abdellatif Helaly [1,*], Heba Sahyon [2], Hala Kiwan [1], Abdel Ghany Shoair [3], Ashraf El-Bindary [1]

[1] Department of Chemistry, Faculty of Science, Damietta University, Damietta 34517, Egypt; abdohelaly@du.edu.eg (A.H.); halakiwan@du.edu.eg (H.K.); abindary@du.edu.eg (A.E.-B.);
[2] Department of Chemistry, Faculty of Science, Kafrelsheikh University, Kafrelsheikh 33516, Egypt; hebasahuon@sci.kfs.edu.eg (H.S.);
[3] Department of Science and Technology, Ranyah University College, Taif University, Saudi Arabia; abdelshoair@yahoo.com (A.S.);
* Correspondence: abdohelaly@du.edu.eg (A.H.);

Scopus Author ID: 57200532999
Received: 26.06.2022; Accepted: 30.07.2022; Published: 7.10.2022

Abstract: Novel 2-aminomethyl benzimidazole (AMBI) ruthenium complexes were synthesized and thoroughly characterized by elemental analysis, spectroscopy (FTIR, 1HNMR, UV–Vis), magnetic measurements, molar conductivity, and thermal analysis techniques. According to analytical data, all complexes demonstrated a 1:1 metal-to-ligand ratio with an octahedral shape. Thermal analysis showed that the complexes have acceptable thermal stability. Cyclic voltammetry was also used to observe their redox actions, and it was found that all of the complexes had electrochemical activity. Using GAUSSIAN 09 W software, the density functional theory (DFT) method and the 3-21G basis set, optimized structures (HOMO & LUMO) of ruthenium complexes (1-4) were carried out. Additionally, the selected quantum and geometric parameters of bond lengths and angles have been determined. The antimicrobial activity of ligand and ruthenium complexes has been evaluated against bacteria (*Escherichia coli*, *Staphylococcus aureus*) and fungi (*Candida albicans*). Two human cancers, HePG-2(hepatocellular carcinoma) and MCF-7 (Michigan Cancer Foundation-7), were tested for cytotoxic activity of complexes. Using the ABTS technique, the antioxidant function of complexes was evaluated. Using a high-affinity Fab sandwich and a specific PCa antibody, molecular docking was utilized to anticipate how the ligand would bind to a human prostate-specific antigen (PSA) immune system receptor (3qum).

Keywords: antibacterial; antioxidant; 2-aminomethyl benzimidazole; complexes; ruthenium.

1. Introduction

Ruthenium complexes are a perfect example of compounds that continue to attract much attention due to their promising function in catalytic and stoichiometric reactions [1, 2]. Ruthenium has also proven to be the most promising metal in potential cancer treatment to replace platinum. Most compounds of ruthenium have low systemic toxicity, and most complexes of Ru(II) and Ru(III) exhibit slow kinetics of ligand exchange, close to those of platinum(II) complexes, which appear to be important for anticancer activity. Besides, ruthenium can accumulate better in cancer cells than platinum [3]. The synthesis and characterization of a number of Ru(II) and Ru(III) complexes containing tertiary phosphines

or arsines have been carried out by various workers [4]. A few of these complexes have been used as good catalysts [5] and some as starting materials [6] for the syntheses of a wide range of Ru(II) complexes containing triphenylphosphine or arsine and other ligand molecules.

As part of an extensive program on the study of metal complexes for the platinum group with bifunctional ligands, we have synthesized some complexes between 2-aminomethyl benzimidazole with Ru(III) and Ru(II). Complexes containing the histidine residue imidazole ring are beneficial model compounds of bioinorganic interest [7,8]. It is also well accepted that the amino group serves as the primary anchor site for metal ions and, as such, is capable of facilitating the deprotonation stepwise and corresponding coordination of other binding sites, leading to the creation of hydrolytically stable, fused, five-membered chelate rings with of M-N bonds. So, metal complexes of various bioligands, known as heteroaromatic nitrogen bases, substrate metal ion enzyme interactions, and other biochemical interactions driven by metal ions, can be regarded as models [9,10]. It has also been shown that 2-aminomethyl benzimidazole (AMBI) is essential because compounds containing this heterocycle exhibit a wide range of pharmacological activities [11], including a variation of antifungal [12], antibacterial [13], antimicrobial[14,15], antiamoebic [16], antiparasitic [17] and antitumor applications [18].

In this article, we study the synthesis and characterization of 2-aminomethyl benzimidazole complexes of Ru(II) and Ru(III). Secondly, DFT studies were carried out for additional information about the molecular structure, bonding nature, and quantum chemical properties. Ligand and resulting complexes have been tested for biological activities (antimicrobial, antifungal, cytotoxic, and antioxidant). Furthermore, Molecular docking has also been used to predict the binding of the 3qum-immune system receptor ligand.

2. Materials and Methods

2.1. Chemicals and reagents.

Hydrated ruthenium trichloride ($RuCl_3 \cdot 3H_2O$/10452), 2-aminomethyl benzimidazole dihydrochloride (AMBI/165638), tetrabutylammonium hexafluorophosphate (TBHFP/281026) were purchased from Sigma-Aldrich and used directly. Other chemicals and solvents were obtained from Fluka and used as received.

2.2. Instrumentation.

Automatic Analyzer CHN Vario ELIII, Germany, obtained microanalytic data (C, H, and N). The following instruments were used to obtain spectroscopic data: FTIR spectra (KBr disks, 4000-400 cm-1) by Jasco FTIR-4100 spectrophotometer; (1H, 13C)NMR spectra by Bruker WP operating at 300 and 75 MHz, using DMSO-d6 as a solvent, respectively. Using tetramethyl silane (TMS) as the internal reference, chemical changes are recorded in ppm; Perkin-Elmer AA800 spectrophotometer Model AAS, UV-Visible spectra, using a 1.0 cm cell. Thermal analysis of the Ru(II/III) complexes was performed using a nitrogen atmospheric Shimadzu thermogravimetric analyzer with a heating rate of 20°C / min over a temperature range of up to 1000°C from room temperature. The conductivity of the complexes at 25 ± 1°C was calculated in DMF (10-3 M) using the conductivity/TDS meter model Lutron YK-22CT. The complexes' electrochemical activity was analyzed in the nitrogen atmosphere and at room temperature using the electrochemical analyzer CHI 610A (HCH Instrument). There are three electrodes in the electrochemical cell used in this work: the platinum wire was used as a

working electrode, Ag+/AgCl was used as a reference electrode, and the platinum wire as a counter electrode. The molecular structures of the ruthenium complexes have been optimized by the 3-21G basis set with DFT methodology using Gaussian 09 W software [19,20]. The molecules were designed with Perkin Elmer ChemBio Draw and optimized using Perkin Elmer ChemBio3D software [21]. The ligand-protein pairwise interaction energies are measured in the docking simulation analysis using Docking Server [22]. Using the Docking Server, Force field MMFF94 was used to reduce ligand molecule energy. The ligand atoms were added to partial charges from Gasteiger. Atoms of non-polar hydrogen have been mixed, and rotatable bonds have been identified. Using Auto Dock software, critical hydrogen atoms, Kollman combined atom-type charges, and solving parameters were added [23]. Affinity (grid) maps were produced using the Autogrid software using 20 × 20 × 20 Å grid points and 0.375 Å spacing [24]. In the Vander Waals measurement and the electrostatic terms, the Auto Dock parameter set and distance-dependent dielectric functions were used, respectively. The Lamarckian genetic algorithm (LGA) and the Solis & Wets local search method were used to conduct docking simulations [25]. The ligand molecules' initial position, orientation, and torsions were randomly set. After a maximum of 250000 energy evaluations, each docking experiment was extracted from 10 separate runs that were set to end. A translational step of 0.2 Å and quaternion and torsion steps of 5 was applied during the process.

2.3. Synthesis of Ru^{II} and Ru^{III} complexes (1-4).

2.3.1. Synthesis of [$Ru^{III}Cl_3$ (AMBI) (H_2O)].

2-aminomethyl benzimidazole (0.220 g, 1 mmol) was dissolved in (20 cm^3) of ethanol $RuCl_3.3H_2O$ (0.261 g, 1 mmol) was dissolved and refluxed in ethanol (20 cm^3) until the initial black color turned into green. The aqueous of the ligand previously prepared was added to this green solution then the reaction mixture was refluxed for 3 h [26]. As a result of refluxing, brown microcrystals were formed, collected by filtration using filtered glass gooch, washed with ethanol (10 cm^3), and dried over anhydrous $CaCl_2$ in a vacuum desiccator (Figure 1). Calcd for $C_8H_{11}Cl_3N_3ORu$ (372.62) (%): C, 25.79; H, 2.98; N, 11.28. Found (%): C, 25.60; H, 2.80; N, 11.50.

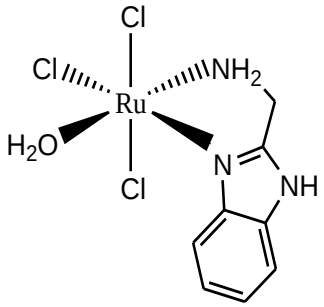

Figure 1. The proposed structure of [RuIIICl3 (AMBI) (H2O)] complex. RuCl3. 3H2O + AMBI → [RuIIICl3 (AMBI)(H2O)].

2.3.2. Synthesis of [$Ru^{III}Cl_2$ ($AsPh_3$)2(AMBI)]2H_2O. CH_3OH.

2-aminomethyl benzimidazole (0.06 g, 0.025 mmol) was dissolved in (20 cm^3) of methanol, then added dropwise to a hot methanol solution (20 cm^3) of [$RuCl_3(AsPh_3)_2$ CH_3OH] (0.2 g, 0.025 mmol) with stirring and the mixture of the reaction was refluxed for 3 h [26]. The solution was concentrated to half of its original volume by evaporation and allowed to cool at

room temperature. During this, a red microcrystalline solid was separated, which was isolated by filtration, washed with hot methanol (10 cm^3), and dried over anhydrous $CaCl_2$ in a vacuum desiccator (Figure 2). The empirical data for this complex is well consistent with its formula. Calcd for $C_{45}H_{46}$ $As_2Cl_2N_3O_3Ru$ (998.6) (%): C, 54.12; H, 4.64; N, 4.21. Found (%): C, 54.38; H, 4.42; N, 4.39.

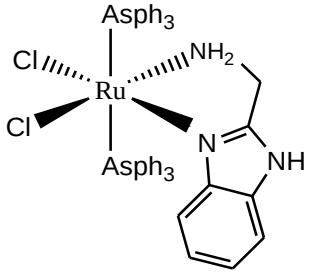

Figure 2. The proposed structure of $[Ru^{III}Cl_2(AsPh_3)_2(AMBI)]2H_2O.\ CH_3OH$. $[RuCl_3(AsPh_3)_2\ CH_3OH]$ + AMBI → $[RuCl_2(AsPh_3)_2(AMBI)].2H_2O.\ CH_3OH$.

2.3.3. Synthesis of $[Ru(bipy)_2(AMBI)](PF_6)_2$.

Under nitrogen, $[RuCl_2(bipy)_2].2H_2O$ (0.13 g, 0.025 mmol) was dissolved in (15ml dist. water,15ml methanol) [26]. 2-aminomethyl benzimidazole (0.03 g, 0.025 mmol) was added to the previous solution with stirring, and the mixture of the reaction was refluxed for 2 h, and then added NH_4PF_6 to the obtained solution. As a result, red microcrystals were formed, which were collected by filtration using filtered glass gooch, washed with hot methanol (10 cm^3), and dried over anhydrous $CaCl_2$ in a vacuum desiccator. The analytical data for this complex are well agreed with its formula, as shown in Figure 3. Calcd for $C_{28}H_{25}$ F_{12} N_7P_2Ru (850.5) (%): C, 39.54; H, 2.96; N, 11.53. Found (%): C, 39.38; H, 2.87; N, 11.61.

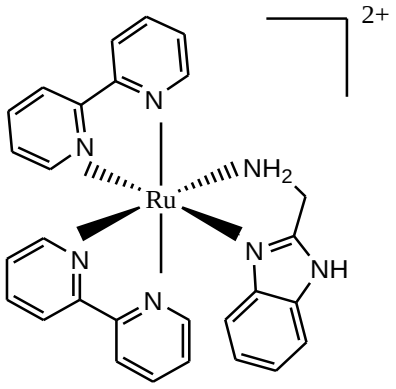

Figure 3. The proposed structure of $[Ru(bipy)_2(AMBI)](PF_6)_2]$ complex. $[RuCl_2(bipy)_2].2H_2O$ + AMBI → $[Ru(bipy)_2(AMBI)](PF_6)_2$.

2.3.4 Synthesis of $[RuCl_2\ (PPh_3)_2(AMBI)]$.

Under nitrogen, $[RuCl_2(PPh_3)_3]$ (0.25 g, 0.025 mmol) was dissolved in 25 ml of methanol. 2-aminomethyl benzimidazole (0.03 g, 0.025 mmol) was added to the previous solution with stirring, and the reaction mixture was refluxed for 2 h [26]. As a result of refluxing, brown microcrystals were formed, which were collected by filtration using filtered glass gooch. Washed with methanol (10 cm^3) and dried over anhydrous $CaCl_2$ in a vacuum desiccator. The analytical data for this complex are well agreed with its formula, as shown in (Figure 4). Calcd for $C_{44}H_{39}$ $Cl_2N_3P_2Ru$ (843.7) (%): C, 62.64; H, 4.66; N, 4.98. Found (%): C, 62.69; H, 4.58; N,4.82.

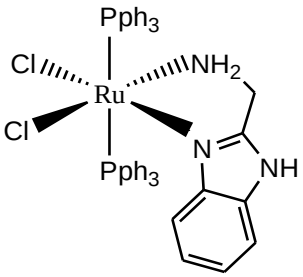

Figure 4. The proposed structure of the [$RuCl_2$ (PPh_3)$_2$(AMBI)] complex. [$RuCl_2$ (PPh_3)$_3$] + AMBI → [$RuCl_2$ (PPh_3)$_2$(AMBI)].

2.4. Antimicrobial investigation.

Each type of bacteria was tested individually against ruthenium complexes, including gram-negative (*Escherichia coli*), gram-positive (*Staphylococcus aureus*), and fungi (*Candida albicans*). Each compound was dissolved in DMSO, and 1 mg/ml concentration solutions were prepared separately, and Whatman filter paper discs of standard size (5 cm) were prepared and sterilized in an autoclave.The paper discs were immersed in the appropriate concentration of the complex solution and then inserted aseptically onto Petri dishes containing nutritional agar media (20 g of agar, 3 g of beef extract, and 5 g of peptone) that had been seeded with *Staphylococcus aureus*, *E. coli*, and *Candida albicans*. Petri dishes were incubated at a temperature of 36°C, and inhibition zones were registered 24 hours after incubation. There were three replications of each treatment. The same procedure was used to report the antibacterial activity of the well-known standard antibiotic ampicillin and the antifungal clotrimazole at the same concentration and solvents. The formula (Eq. 1) was used to get the complex's percentage activity index.

$$\% \text{ Activity Index} = \frac{\text{Zone of inhibition by test compound (diameter)}}{\text{Zone of inhibition by standard (diameter)}} \times 100 \quad (1)$$

2.5. Cytotoxicity investigation.

2.5.1. Cell lines and chemical reagents.

Breast cancer of the mammary gland (MCF-7) and hepatocellular carcinoma (HePG-2) cell lines were collected from ATCC through the Biological Products and Vaccines Holding Company (VACSERA) of Cairo, Egypt. Chemical reagents were purchased from Sigma Company (St. Louis, USA), Fetal Bovine Serum (FBS) was purchased from (GIBCO, UK), RPMI-1640 medium, MTT, DMSO, and doxorubicin. As a typical anticancer drug for comparison, doxorubicin was used.

2.5.2. MTT assay.

Using the MTT test, the cell lines described above have been used to assess the compounds' inhibitory effects on cell growth [27]. This colorimetric assay is based on conversion by mitochondrial succinate dehydrogenase in viable yellow tetrazolium bromide (MTT) cells to a purple formazan derivative. With 10 percent fetal bovine serum, cell lines were cultured in RPMI-1640 medium. In a 5 percent CO_2 incubator, the antibiotics added were 100 units/ml and 100µg / ml streptomycin at 37°C. The cell lines were seeded for 48 h and under 5% CO_2 in a 96-well plate at a density of 11.0x104 cells/well at 37°C.

The cells were treated after being incubated for 24 hours at varying doses of compounds. [28]. Following the drug treatment, 20 µl of MTT solution containing 5 mg/ml was added and incubated for 4 hours. Dimethyl sulfoxide (DMSO) of 100 µL volume is added to each well to dissolve the formed purple formazan. Using a plate reader, the colorimetric assay is recorded as absorbance at 570 nm (EXL 800, USA). Cytotoxicity was expressed as IC50 (µg/mL), suggesting the compound's concentration inhibited the tumor cells' proliferation rate by 50 % compared to untreated control cells. IC50 values were determined from the plot: percent relative cell viability (inhibition concentration percent) versus compound concentration. The relative cell viability values were calculated as follows (Eq. 2):

$$\%\ \text{The relative cell viability} = \frac{\text{A (570 nm) of treated samples}}{\text{A (570 nm) of untreated sample}} \times 100 \quad (2)$$

2.6. Antioxidant investigation.

L-Ascorbic acid was obtained from Sigma, ABTS was purchased from Wak (2,2'-azinobis-(3-ethyl-benzothiazoline-6-sulphonic acid), and all other chemicals were of the highest available quality. The ABTS method [29] antioxidant activity screening assay was used to assess compounds' scavenging activity. ABTS solution (60 µM) was applied to 3 mL of MnO_2 solution (25 mg/mL) for each of the examined compounds (2 mL). Every single one was made in a 5 mL aqueous phosphate buffer solution (pH 7, 0.1 M). After shaking, centrifuging, and filtering the mixture, the absorbance of the resulting green-blue solution (ABTS free radical solution) at 734 nm was set to approximately ca. 0.5. The tested compound (50 µl, mM) in a spectroscopic grade CH_3OH/phosphate buffer (1:1) was added. The absorbance was read, and the percentage of inhibition (I percent) was used to express the color intensity reduction as illustrated in (Eq. 3). Instead of the tested compounds, a blank sample containing only CH_3OH/phosphate buffer (1:1) was run without ABTS. L-ascorbic acid was used as a normal antioxidant (positive control), and only ABTS and CH_3OH / phosphate buffer (1:1) was used for negative control.

$$\%\ \text{Inhibition} = \frac{\text{A (control)} - \text{A (test)}}{\text{A (control)}} \times 100 \quad (3)$$

3. Results and Discussion

3.1. Characterization of ruthenium complexes.

The analytical data from the complexes Ru(II) and Ru(III) showed that the complexes have a stoichiometry of 1:1 (metal: ligand). Dimethylformamide (DMF) is used to calculate the molar conductance values for ruthenium complexes (10^{-3} M).

Table 1. Physical properties and elemental analysis data of Ru(II) and Ru(III) complexes.

Complex	Color	M.P. (°C)	% Calcd. (Found)		
			C	H	N
$[RuCl_3(AMBI)(H_2O)]$	Brown	>360	25.79(25.60)	2.98(2.80)	11.28(11.50)
$[RuCl_2(AsPh_3)_2(AMBI)].2H_2O.CH_3OH$	Dark red	200	54.06(54.38)	4.74(4.42)	4.20(4.39)
$[Ru(bipy)_2(AMBI)](PF_6)_2$	Red	270	39.54(39.38)	2.96(2.87)	11.53(11.61)
$[RuCl_2\ (PPh_3)_2(AMBI)]$	Brown	190	62.64(62.69)	4.66(4.58)	4.98(4.82)

The values for the complexes (1,2,3,4) were found to be 7, 2, 6, 150 Ω−1cm^{2}mol^{-1}, respectively, indicating that the complexes (1,2,3) are non-electrolytes, while the complex (4) is an electrolyte. The formulation of the synthesized complexes is based on elemental analysis, molar conductance, IR, UV-Visible, and ^{1}HNMR spectroscopy. In Table 1, the physical properties and analytical data are shown.

3.2. Infrared spectra.

The ligand's coordination modes to ruthenium complexes were assigned through a comparison of the infrared spectra of the Ru(II), Ru(III) complexes with the spectra of the free ligand. IR spectra have proved to be the most effective approach to provide sufficient details to elucidate the ligands' way of bonding to the metal ions. Table 2 summarizes the major IR bands with their approximate assignments. The free AMBI ligand infrared spectrum reveals one medium and broad absorption band in the region of 3348-3270 cm^{-1}, stretching vibrations of the (-NH2) groups and showing one stretching band at 1628 cm^{-1}, indicating the vibration of the imidazole ring tertiary nitrogen atom (-N= CH-)**.** In addition, the ligand displays a single sharp and solid band characteristic of the stretching ν(C=N) vibration [30] at 1628 cm^{-1}. This band undergoes a negative shift in the complexes suggesting azomethine nitrogen's involvement in coordination. The IR spectra of the free ligand typically show a large band of about 3050 cm^{-1} which can be due to the benzimidazole moiety's -NH stretching vibration. In addition, the presence of two medium-intensity bands in the ligand and the complexes in regions 3128-3396 and 3207-3410 cm^{-1} suggests the involvement of the NH_2 group in the coordination. The other M-N band appears at approximately 430 cm^{-1} [31].

Table 2. Tentative allocation of the ligand's essential infrared bands and their synthesized complexes.

	Compound	Assigned wave numbers (cm^{-1})			
		ν(NH_2)	ν(–N=C–)	ν(-NH)	ν(Ru-N)
	Ligand (AMBI)	3270 -3348	1628	3050	-
1	[$RuCl_3$(AMBI)(H_2O)]	3390 -3410	1620	3057	416
2	[$RuCl_2$($AsPh_3$)$_2$(AMBI)]2H_2O.CH_3OH	3128 -3207	1580	3053	451
3	[Ru(bipy)$_2$(AMBI)](PF_6)$_2$	3396 -3405	1608	3055	443
4	[$RuCl_2$ (PPh_3)$_2$(AMBI)]	3335 -3370	1570	3053	452

3.3. Magnetic and electronic spectral measurements.

Magnetic susceptibility was measured at 298 K for the solid complexes. The paramagnetic complex (1, 2) corresponds to one unpaired electron with μ_{eff} values of 1.67 and 1.9 BM, respectively. This close spin-only value (1.73 BM) is predicted for a low spin S= 1⁄2 configuration of 4d5 (t_2g5) as is usual for the ruthenium (III) complex in an octahedral setting [30].

Diamagnetic and EPR silent compliant with d0 configuration was found for the other complexes(3,4).

Electronic spectra bands of the ruthenium complexes were performed in CH_2Cl_2 or DMF (10−3-10−5 M) concentrations in the region of 200–900 nm. The spectral data were collected in Tables 3, and 4, and illustrated in Figure 5. Electronic spectrum bands of complexes below 400 nm assigned to intra-ligand (AMBI) charge transfer: π–π* and n–π* transitions, respectively [33]. Besides these bands, the spectrum showed a third intense absorption band near 550 nm, which can be assigned to charge transfer transitions [34]. D-d transitions are assigned to the weak bands of complexes seen in the visible field [35].

Table 3. Electronic spectral data of ruthenium complexes.

	Complex	Solvent	Electronic spectral bands (nm)	Assignment
1	$[RuCl_3(AMBI)(H_2O)]$	DMF	370	π–π*
			383	n–π*
			575	LMCT
2	$[RuCl_2(AsPh_3)_2(AMBI)].2H_2O.CH_3OH$	CH_2Cl_2	325	π–π*
			372	n–π*
			450	LMCT
3	$[Ru(bipy)_2(AMBI)](PF_6)_2$	DMF	355	n–π*
			500	MLCT
			630	d–d
4	$[RuCl_2(PPh_3)_2(AMBI)]$	CH_2Cl_2	395	n–π*
			477	MLCT
			620	d–d

Table 4. Cyclic voltammetric data for the Ru(II) and Ru(III) complexes.

Complex	$E_{pa(V)}$	$E_{pc(V)}$	$\Delta E_{(V)}$	$E_{½(V)}$	Assignment
(1)	1.27	1.150	0.120	1.21	Ru^{III} / Ru^{IV} or Ru^{V}
(2)	1.08	0.800	0.280	0.94	Ru^{III} / Ru^{IV} or Ru^{V}
(3)	1.3	0.825	0.475	1.0625	Ru^{II}/Ru^{III}
(4)	1.025	0.725	0.300	0.875	Ru^{II}/Ru^{III}

Conditions: supporting electrolyte (0.2 g, TBHFP), the concentration of the complex; ~10 -3M, $\Delta E = E_{pa}$-E_{pc} and $E_{1/2} = 0.5$ (E_{pa}+ E_{pc}), where E_{pa} and E_{pc} are the anodic and cathodic cyclic voltammetric peak potentials.

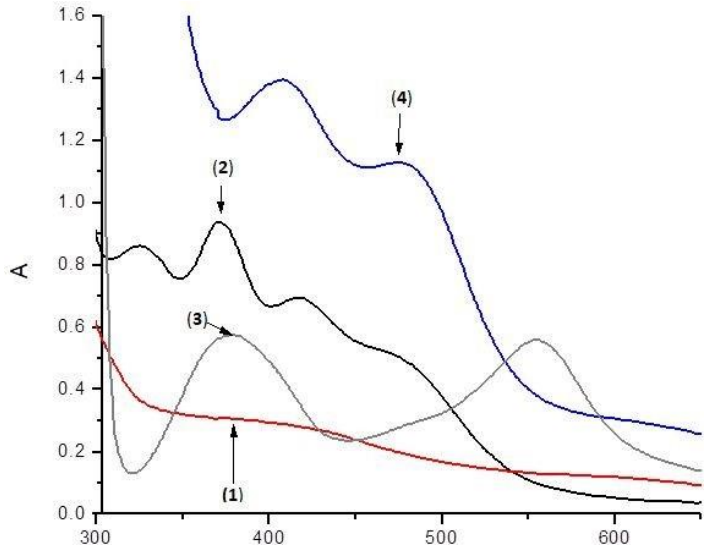

Figure 5. Electronic spectra of complexes (1-4).

3.4. Electrochemical properties of Ru(II) and Ru(III) complexes.

All ruthenium complexes' electrochemical properties were investigated by cyclic voltammetry in DMF solvent containing (0.2 g TBHFP) as the supporting electrolyte. Voltammetric data are presented in Table 4, and a selective voltammogram is shown in Figure 6. The voltammogram of all complexes (1-4) illustrates no exception concerning their electrochemical behavior. The complexes (1,2) demonstrated one irreversible oxidation wave on the positive side of the Ag+/AgCl electrode (ΔE = 120, 280 mV) due to the oxidation of RuIII to a higher oxidation state RuIV or RuV. Whereas under the same conditions, the complexes (3,4) illustrated one irreversible oxidation wave on the positive side of the Ag+/AgCl electrode (ΔE = 300, 475 mV) respectively attributable to oxidation of Ru(II) to Ru(III). The irreversibility of these complexes may be due to their high stability.

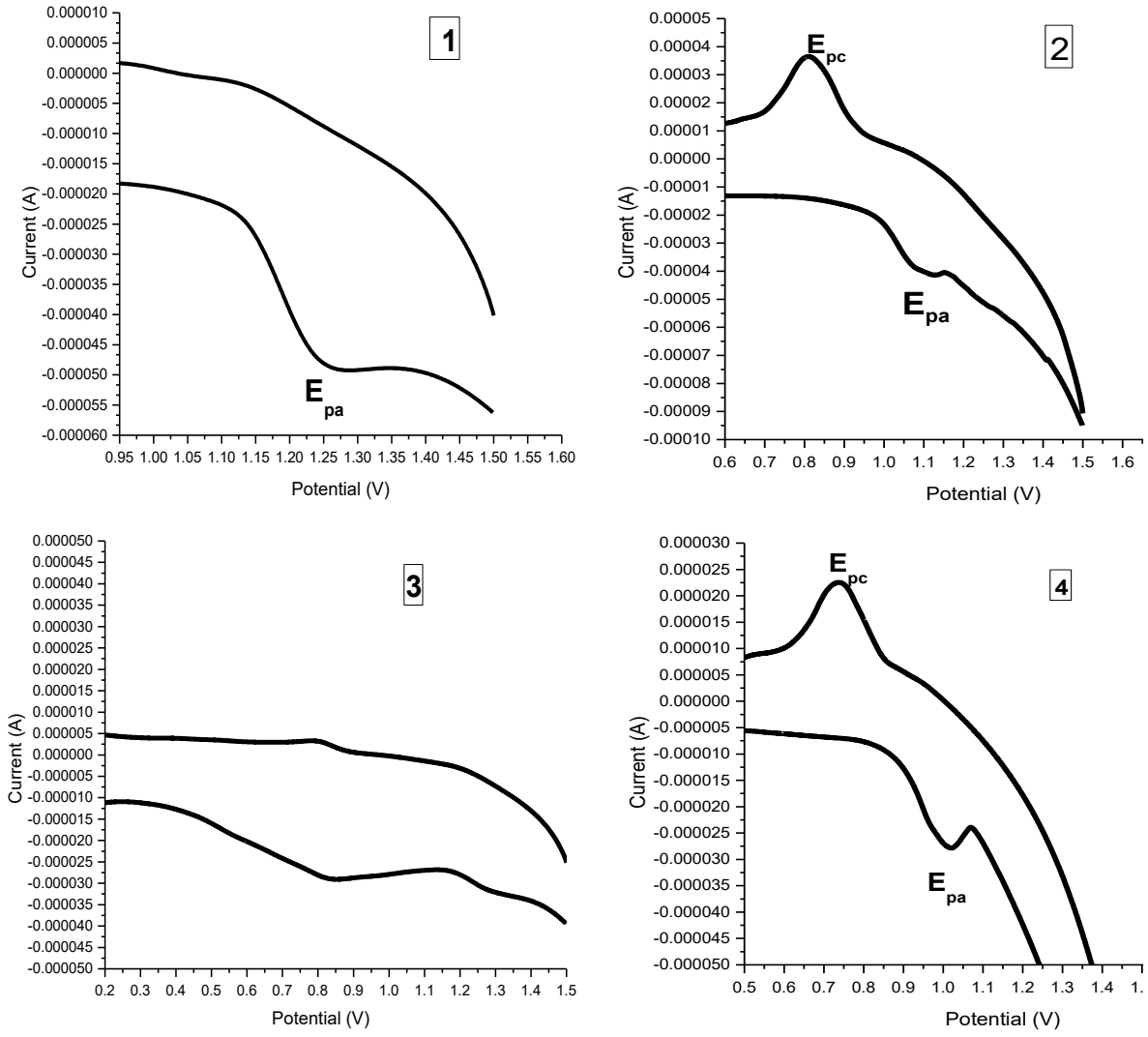

Figure 6. Cyclic voltammogram complexes.

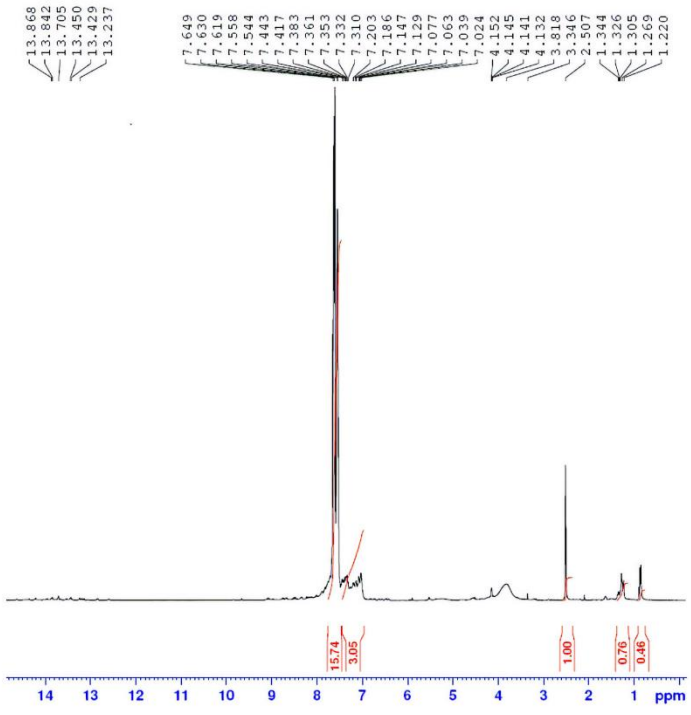

Figure 7. ^{1}HNMR spectrum of [$RuCl_2$ (PPh_3)$_2$(AMBI)].

3.5. [1]HNMR spectrum.

The 1HNMR spectra of the Ru(II) complexes were recorded in DMSO-d6 at room temperature using tetramethyl silane (TMS) as the standard shown in Figure 7. The singlet peak at δ 0.8 ppm corresponds to the NH proton, while the singlet peak at δ 1.2 ppm is related to the two protons of the NH_2 group. The singlet peak at δ 2.5 ppm is related to the two protons of the CH_2 group, the Multiplet peak at δ 7.2 ppm is related to the aromatic protons of the benzimidazole ring, and the Multiplet peak at δ 7.6 ppm is related to the aromatic protons of phenyl groups.

3.6. Molecular structure.

The molecular structures of ruthenium complexes (1-4) (HOMO & LUMO) are shown in Figures 8 and 9, and the selected geometric parameters are described in Tables S1, S2, S3, and S4 of the Supplementary file. The estimated quantum chemical parameters are provided in Table 9. [36]. In many molecular systems, the HOMO-LUMO energy gap (E) is a significant stability index that is used to generate theoretical models to explain the structure and conformational barriers [37]. The ΔE values of ruthenium complexes show that complex (2) is more stable than the other complexes [38]. Additional parameters such as separation energies, ΔE, absolute electronegativity, χ, chemical potentials, Pi, absolute hardness, η, absolute softness, σ, global electrophilicity, ω, global softness, S, and additional electronic charge, ΔN_{max}, were determined in accordance with the following Eqs. (4–11):

$$\Delta E = E_{LUMO} - E_{HOMO} \quad (4)$$

$$\chi = \frac{-(E_{HOMO} + E_{LUMO})}{2} \quad (5)$$

$$\eta = \frac{E_{LUMO} - E_{HOMO}}{2} \quad (6)$$

$$\sigma = 1/\eta \quad (7)$$

$$Pi = -\chi \quad (8)$$

$$S = \frac{1}{2\eta} \quad (9)$$

$$\omega = Pi^2 / 2\eta \quad (10)$$

$$\Delta N_{max} = -Pi/\eta \quad (11)$$

HOMO **LUMO**

1)

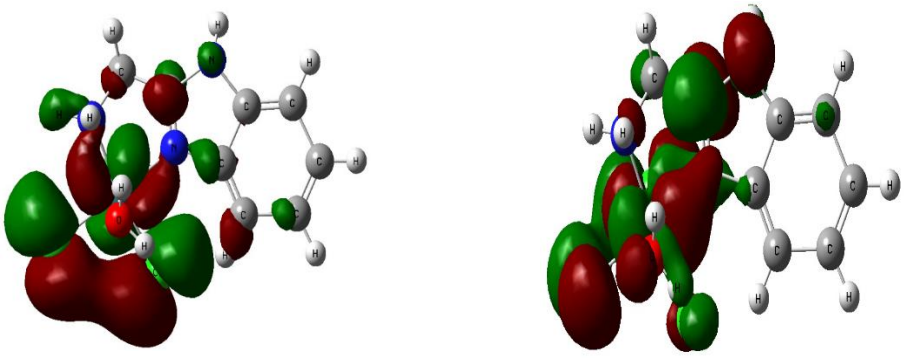

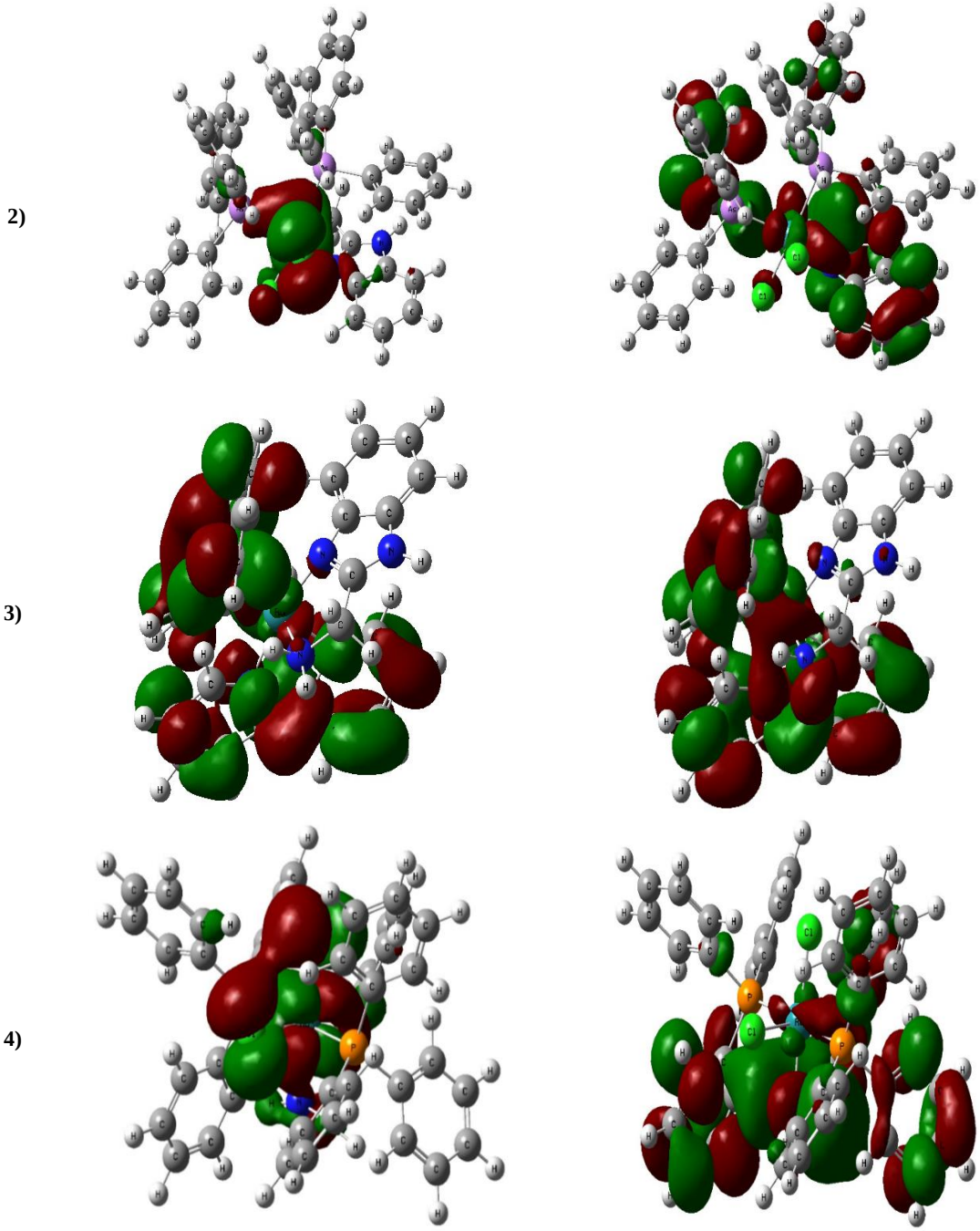

Figure 8. The highest occupied Molecular orbital (HOMO) and the lowest unoccupied molecular orbital (LUMO) of ruthenium complexes (1–4).].

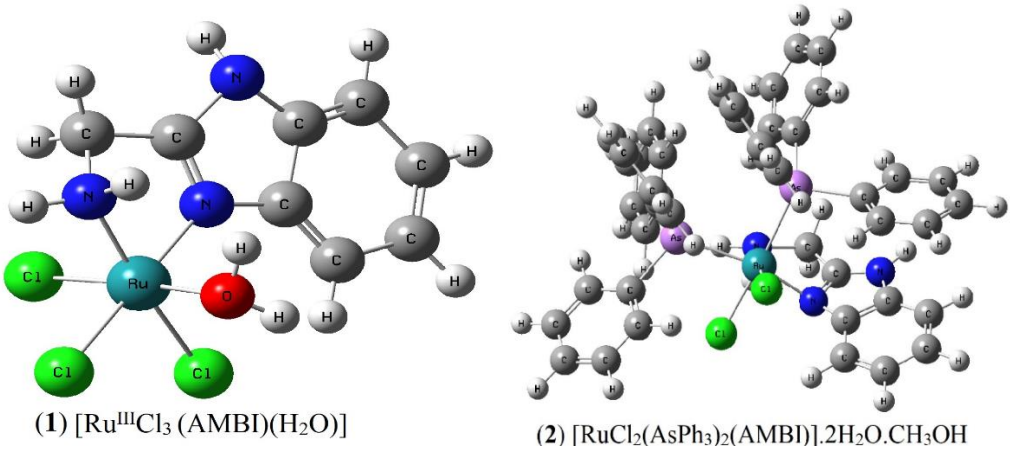

(**1**) $[Ru^{III}Cl_3(AMBI)(H_2O)]$ (**2**) $[RuCl_2(AsPh_3)_2(AMBI)].2H_2O.CH_3OH$

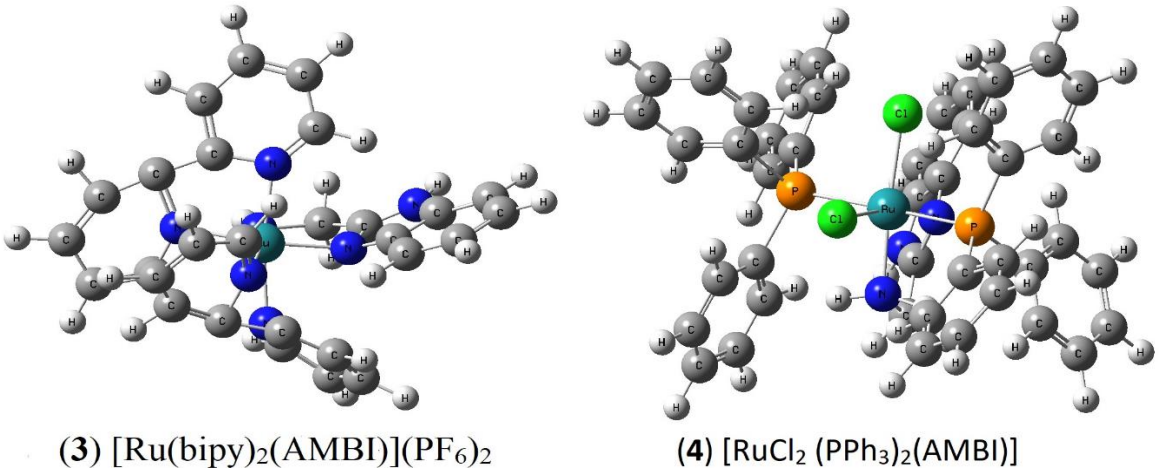

(3) $[Ru(bipy)_2(AMBI)](PF_6)_2$ (4) $[RuCl_2(PPh_3)_2(AMBI)]$

Figure 9. The calculated molecular structures of ruthenium complexes (1–4).

Table 9. The calculated quantum chemical properties of ruthenium complexes (1-4).

	-EHOMO (a.u.)	-ELUMO (a.u.)	ΔE (a.u.)	χ (a.u.)	η (a.u.)	σ (a.u.)-1	- Pi (a.u.)	S (a.u.)-1	ω (a.u.)	Δ*N*max (a.u.)
1)	0.186	0.114	0.072	0.15	0.036	27.778	0.15	13.889	0.313	4.167
2)	0.138	0.026	0.112	0.082	0.056	17.857	0.082	8.929	0.060	1.464
3)	0.0723	0.047	0.025	0.059	0.013	79.051	0.059	39.526	0.141	4.715
4)	0.12244	0.027	0.095	0.075	0.048	21.064	0.075	10.532	0.059	1.579

3.7. Thermal analyses.

For the complexes, the TGA curves indicate that the substituent change affects the complexes' thermal properties. Table 10 lists the temperature intervals and the percentage of mass loss.

Table 10. The thermal analysis data for Ru(II) and Ru(III) Complexes.

Complex	Temp. range (°C)	Found mass loss(calc.) %	Assignment
$[RuCl_3(AMBI)(H_2O)]$	100-360	33.32 (33.38)	Loss of H_2O +3Cl
	360-470	35.73 (35.74)	Loss of $C_8H_9N_2$
	>470	30.95 (30.88)	Loss of RuN
$[RuCl_2(AsPh_3)_2(AMBI)].2H_2O.CH_3OH$	100-200	6.82 (6.80)	Loss of $2H_2O$ +MeOH
	200-370	37.70 (37.73)	Loss of Cl_2+$AsPh_3$
	370-600	30.58 (30.63)	Loss of $AsPh_3$
	>600	24.90 (24.84)	Loss of RuN+ $C_8H_8N_2$
$[Ru(bipy)_2(AMBI)](PF_6)_2$	90-270	34.12 (34.09)	Loss of $(PF_6)_2$
	270-540	36.70 (36.73)	Loss of$(bipy)_2$
	540-800	15.62 (15.65)	Loss of $C_8H_9N_2$
	> 800	13.56 (13.53)	Loss of RuN
$[RuCl_2(PPh_3)_2(AMBI)]$	170-410	39.40 (39.49)	Loss of Cl_2+PPh_3
	410-500	31.12 (31.09)	Loss of PPh_3
	> 500	29.48 (29.42)	Loss of RuN+$C_8H_9N_2$

$[RuCl_3(AMBI)(H_2O)]$ complex shows three decomposition steps. The first stage in the temperature range of 100-360°C corresponds to a loss of H_2O and three chloride ions (Found 33.32 %, calc. 33.38 %). The second stage in the temperature range 360-470°C corresponds to a loss of a part of the complex($C_8H_9N_2$) (Found 35.73 %, calc. 35.74%). The final weight loss is due to the ruthenium nitride residue.

$[RuCl_2(AsPh_3)_2(AMBI)]2H_2O.CH_3OH$ complex shows four decomposition steps. The first stage occurs in the temperature range of 100-200°C and is attributed to a loss of two molecules of H_2O and one molecule of CH_3OH (Found at 6.82% and calc. 6.80 %). The second stage in the temperature range 200-370 °C corresponding to loss of $2Cl^- + AsPh_3$ (Found 37.70 %, calc. 37.73%). The third stage in the temperature range 370-600°C corresponds to a loss of $AsPh_3$ (Found at 30.58 %, calc. 30.63%). The final weight loss is due to the rest of the complex and ruthenium nitride residue.

$[Ru(bipy)_2(AMBI)](PF_6)_2$ complex shows four decomposition steps. The first stage occurs in the temperature range of 90-270°C and is attributed to a loss of $(PF_6)_2$ (Found at 34.12 % and calc. 34.09%). The second stage in the temperature range 270-540°C corresponds to a loss of $(bipy)_2$ (Found 36.70 %, calc. 36.73 %). The third stage in the temperature range 540-800°C corresponds to a loss of $C_8H_9N_2$ (Found at 15.62 %, calc. 15.65%). The final weight loss is due to ruthenium nitride residue.

$[RuCl_2(PPh_3)_2(AMBI)]$ complex shows three decomposition steps. The first stage occurs in the temperature range of 170-410 °C and is attributed to a loss of $2Cl^- + PPh_3$ (Found at 39.40 % and calc. 39.49%). The second stage, in the temperature range of 410-500°C, corresponds to a loss of PPh_3 (Found at 31.12 %, calc. 31.09%). The final weight loss is due to the rest of the complex and ruthenium nitride residue.

3.8. Molecular docking.

Cancer can be characterized by cell differentiation arrest, apoptosis inhibition, and accelerated cloned cell proliferation [39,40]. Understanding the cell death execution mechanisms and their role in various diseases opens up new therapeutic strategies [39]. In prostate cancer (PCa) and other prostate diseases, the human prostate-specific antigen (PSA or human kallikrein-related peptidase 3) in small amounts in healthy males' serum is elevated. The ability to recognize the PCa-associated free PSA fraction could improve the reliability of the diagnostic PSA test [41,42]. The main instrument in computational drug design is molecular docking [43]. Molecular docking focuses on simulating the mechanism of molecular recognition. Molecular docking attempts to achieve an optimal protein and drug conformation with relative orientation between them, reducing the total system's free energy. In this work, we used molecular docking between the ligand (AMBI) and prostate cancer (3qum). The findings suggested a potential arrangement between ligand (AMBI) and 3qum receptor.

A favorable interaction between ligand (AMBI) and receptor 3qum was seen in the docking analysis (Figure 10), and the measured energy is shown in Table 11. According to the results obtained in this analysis, the HB plot curve indicates that there were decomposed interaction energies in kCal/mole between ligand (AMBI) with 3qum receptor (Figure 11) binding to the protein with hydrogen bond interactions and decomposed interaction energies in kCal/mole.

When AutoDock's estimated Ki values are compared to accessible experimental Ki values and the Gibbs free energy is negative, the estimated efficiency is advantageous. Based on this evidence, we may also suggest that it is possible to interact between the 3qum receptor and the ligand (AMBI). 2D plot curves of ligand docking (AMBI) are shown in Figure 12. This interaction could cause apoptosis in cancer cells' ligand interaction energy (AMBI). Binding energies are most commonly used as a way to calculate compounds' binding affinity. Thus, the reduction in binding energy due to mutation would increase the compounds' binding affinity towards the receptor. The characteristic features of compounds were represented in the

presence of active sites available for hydrogen bonding. This role allows them to be good protein-binding inhibitors and develop increased inhibitory compounds. Ligand (AMBI) showed -4.58 kCal/mol binding energy, with H-bond, electrostatic, and Vander Waals interacting ions for 3qum receptor prostate cancer. It was deciphered that ligands (AMBI) may be promising inhibitors of 3qum-immune system prostate cancer based on complex scoring and interactions with the active site residue and binding capacity.

Table 11. Energy values obtained in docking calculations of ligands (AMBI) with receptor prostate cancer 3qum.

Compound	Gibbs free energy of binding (kCal/mol)	Inhibition constant (K_i) (uM)	vdW+ H-bond+ desolv energy (kCal/mol)	Electrostatic Energy (kCal/mol)	Total intermolecular Energy (kCal/mol)	Interact surface
(AMBI)	-4.58	439.83	-5.09	-0.25	-5.34	434.992

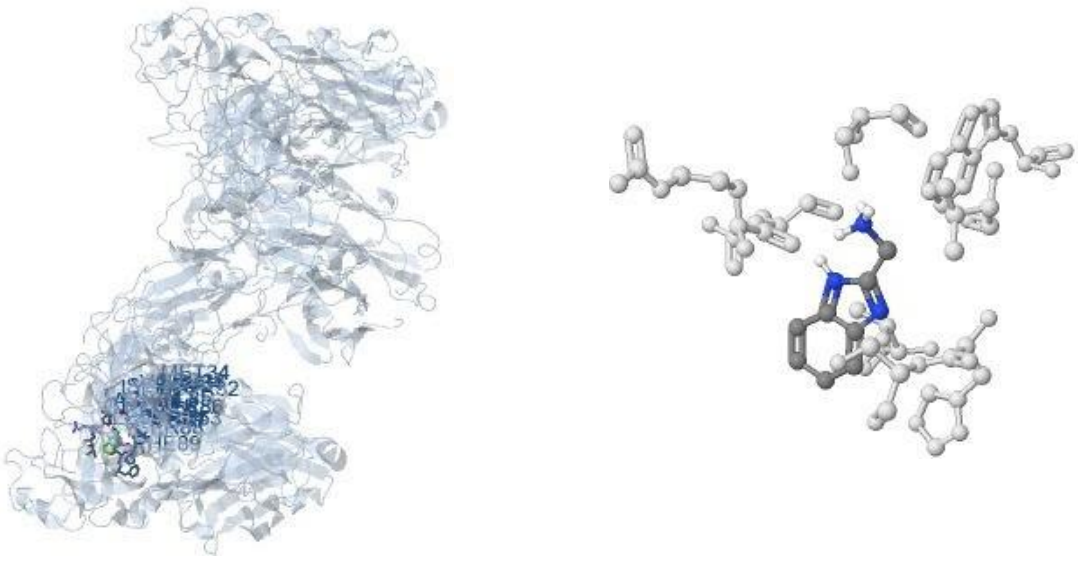

(a) (b)

Figure 10. The ligand (AMBI) (green in (**a**) and blue in (**b**)) interaction with receptor prostate cancer 3qum.

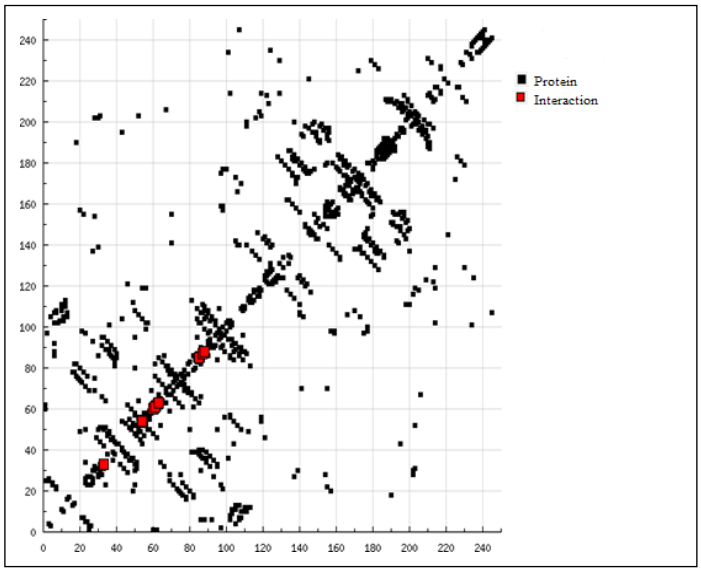

Figure 11. HB plot of interaction between ligand (AMBI) with receptor prostate cancer 3qum.

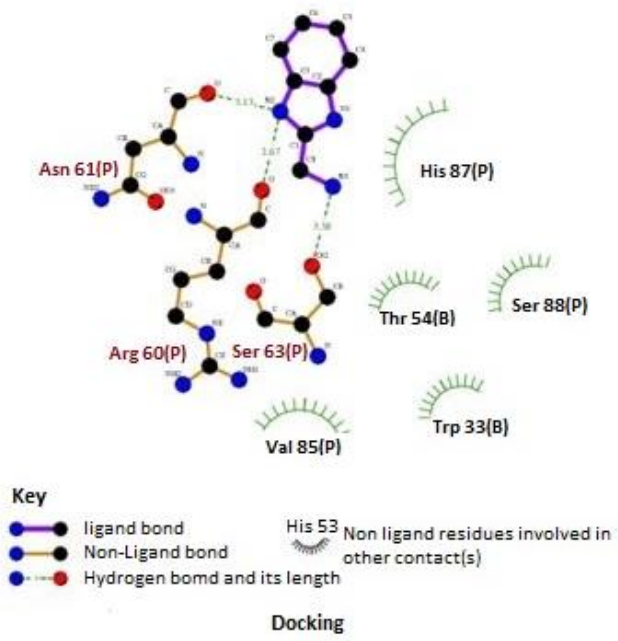

Figure 12. 2D plot of interaction between ligand AMBI with receptor prostate cancer 3qum.

3.9. Antimicrobial activity.

In order to identify a compound's antibacterial properties, it was tested against bacteria and fungi [44]. In the current studies, gram-negative (*Escherichia coli*), gram-positive (*Staphylococcus aureus*), and fungi (*Candida albicans*) species were examined . Table 12 lists the outcomes of the produced compounds' antibacterial activity.

All complexes were found to have antibacterial activity against *Escherichia coli* except Complexes (3,4) (inhibition zone = 11 mm with activity index 44 % for AMBI, inhibition zone = 9 mm with activity index 36 % for Complex (2) and inhibition zone = 4 mm with activity index 16% for Complex (1).

All complexes under investigation have antibacterial activity against *Staphylococcus aureus* except Complex (1) (inhibition zone = 5 mm with activity index 21.7 % for Complex (4),inhibition zone = 17 mm with activity index 73.9 % for AMBI , inhibition zone = 14 mm with activity index 60.9 % for Complex (2) and inhibition zone = 2 mm with activity index 8.7 % for Complex (3).

All complexes under investigation have antifungal activity against *Candida albicans* except complex (1) (inhibition zone = 10 mm with activity index 38.5 % for complex (4), inhibition zone = 8 mm with activity index 30.8 % for AMBI, inhibition zone = 15 mm with activity index 57.7 % for complex (2), inhibition zone = 3 mm with activity index 11.5 % for complex (3). It was found that complex (2) is the highest antifungal activity against *Candida albicans.*

Table 12. The antibacterial and antifungal activities of the ligand and its Ru(II), and Ru(III) complexes.

	E. coli		***S. aureus***		***C. albicansns***	
Complex	**Diameter of inhibition zone (in mm)**	**% Activity index**	**Diameter of inhibition zone (in mm)**	**% Activity index**	**Diameter of inhibition zone (in mm)**	**% Activity index**
(AMBI)	11	44.0	17	73.9	8	30.8
(1)	4	16.0	NA	----	NA	----
(2)	9	36.0	14	60.9	15	57.7
(3)	NA	----	2	8.7	3	11.5

Complex	*E. coli*		*S. aureus*		*C. albicansns*	
	Diameter of inhibition zone (in mm)	% Activity index	Diameter of inhibition zone (in mm)	% Activity index	Diameter of inhibition zone (in mm)	% Activity index
(4)	NA	----	5	21.7	10	38.5
Ampicillin	25	100	23	100	NA	----
Colitrimazole	NA	----	NA	----	26	100

3.10. Cytotoxic activity.

The complexes were tested for in vitro cytotoxic activity against two human cancer cell lines; HePG-2 and MCF-7. Different doses of the investigated compounds (i.e., 100, 50, 25, 12.5, 6.25, 3.125, 1.56, and 0 g) were used to identify inhibitory action against the HePG-2 and MCF-7 cell lines, and the vitality cells (%) was calculated using the colorimetric method, which demonstrated in (Fig. 12). Additionally, Table 13 shows the inhibitory concentration 50 (IC50), which was estimated. Complex (2) had excellent cytotoxic action against the HePG-2 and MCF-7 cell lines, according to the results (IC50 values of 10.20 g/mL and 9.70 g/mL, respectively). Additionally, the ligand has very good cytotoxic properties against the HePG-2 and MCF-7 cell lines (IC50 = 7.90 g/mL and 19.63 g/mL, respectively). Against both (HePG-2) and (MCF-7) cell lines, complexes (3,4) demonstrate good cytotoxic activity, but complex (1) exhibits weak cytotoxic activity. Comparing the doxorubicin response, results indicated that complex (2) has the highest cytotoxic activity than the other complexes.

Table 13. Inhibition of ligand and complexes' cell viability against HePG-2 and MCF-7 cells compared with standard doxorubicin (DOX).

Compounds	*In vitro* Cytotoxicity IC50 (µg/ml)•	
	HePG2	MCF-7
DOX	4.50±0.3	4.17±0.2
$[RuCl_2(PPh_3)_2(L)]$	29.80±2.4	11.66±1.4
AMBI	7.90±0.8	19.63±1.8
$[RuCl_2(AsPh_3)_2(L)].2H_2O.CH_3OH$	10.20±1.2	9.70±1.0
$[RuCl_3(L)(H_2O)]$	63.56±4.1	54.12±3.7
$[Ru(bipy)_2(L)](PF_6)_2$	39.85±2.9	45.93±3.4

Data presented as mean ± SD. IC_{50} (µg/ml): 1 – 10 (very strong). 11 – 20 (strong). 21 – 50 (moderate). 51 – 100 (weak) and above 100 (non-cytotoxic).

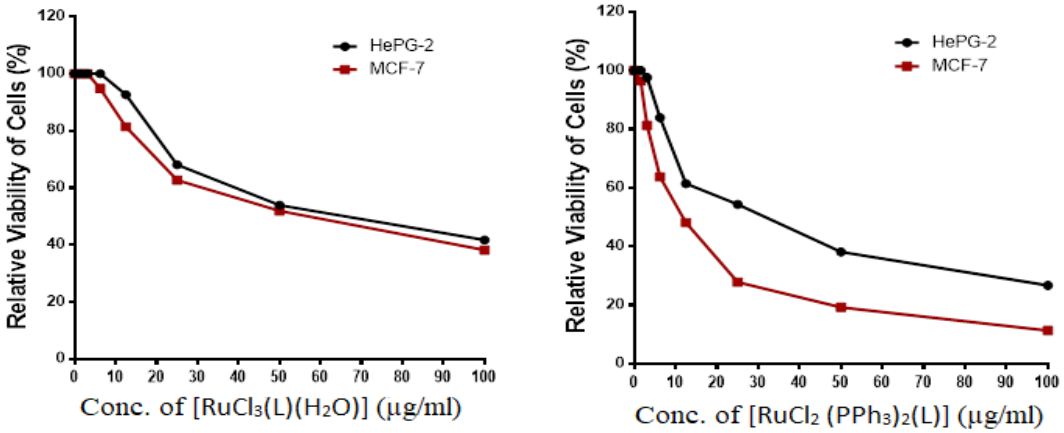

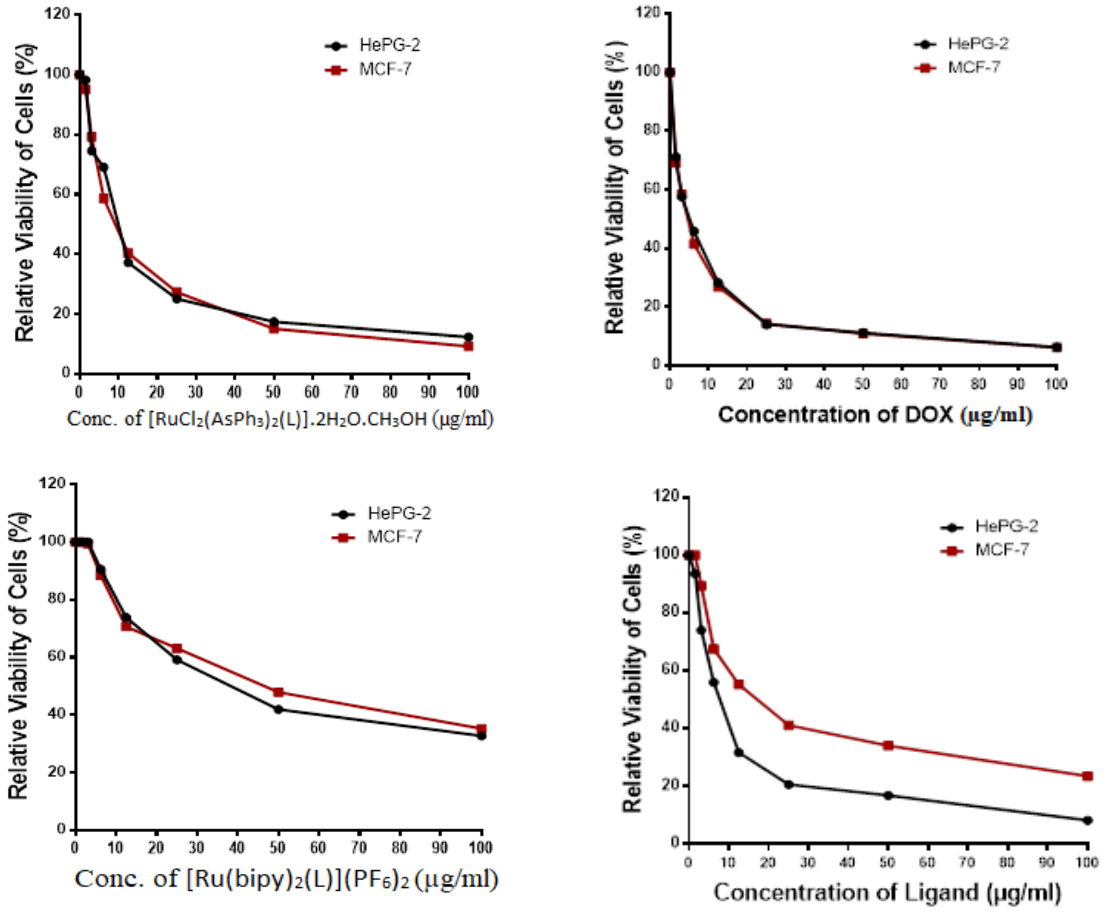

Figure 13. Relative viability cells (%) of ruthenium complexes.

3.11. Antioxidant activity.

Antioxidants are chemical compounds that give the free radical an electron and turn it into a harmless molecule. They can reduce the energy of free radicals, stop the generation of new radicals, stop the broken chain from spreading, heal damage, and rebuild membranes [45]. Results of the ABTS method for each compound and standard ascorbic acid as a reference compound were shown in Table 14, as well as the percentage of inhibition and radical scavenging ability.

Table 14. Results of radical scavenging activity and % of inhibition of each complex and AMBI by ABTS method.

Method	**ABTS** **Abs(control)-Abs(test)/Abs(control)X100**	
Complex	Absorbance of samples	% Inhibition
Control of ABTS	0.495	0
Ascorbic-acid	0.056	88.7%
Ligand (L)	0.294	40.6%
(1)	0.331	33.1%
(2)	0.276	44.2%
(3)	0.325	34.3%
(4)	0.285	42.4%

The results showed that all complexes have good antioxidant activity complex (4) (% inhibition value = 42.4 %), AMBI (% inhibition value = 40.6%), complex (2) (% inhibition

value = 44.2%), complex (1) (% inhibition value = 33.1 %) and complex (3) (% inhibition value = 34.3 %).

4. Conclusions

Four novel ruthenium complexes of 2-aminomethyl benzimidazole were prepared and characterized by Physico-chemical studies. The study reveals that, regarding molar conductivity, RuII and RuIII complexes are mostly non-electrolytes; 2-Aminomethyl benzimidazole ligand behaves as a bidentate ligand and is coordinated through the tertiary nitrogen atom of imidazole ring; the nitrogen atom of the amino group ruthenium complexes have octahedral geometry. The antioxidant and cytotoxic activity of RuII complexes is better than RuIII complexes.

Funding

This research received no external funding.

Acknowledgments

No support was given, which is not covered by the authors' contribution.

Conflicts of Interest

The authors declare no conflict of interest.

References

1. Rao, J; Zhao, J; Zhu, X; Guo, Z; Wang, C; Zhou, C-Y. Rhodium-Catalyzed Reaction of Diazoquinones with Allylboronates to Synthesize Allylphenols. *Org Chem Front* **2022**, https://doi.org/10.1039/D2QO00626J.
2. Singh, P; Kumar Chouhan, K; Mukherjee, A. Ruthenium Catalyzed Intramolecular C−X (X=C, N, O, S) Bond Formation via C−H Functionalization: An Overview. *Chem - An Asian J* .**2021**, 16, 2392–2412, https://doi.org/10.1002/asia.202100513.
3. Scattolin, T; Voloshkin, VA; Visentin, F; Nolan, SP. A Critical Review of Palladium Organometallic Anticancer Agents. *Cell Reports Phys Sci* .**2021**, 2, 100446, https://doi.org/10.1016/j.xcrp.2021.100446 .
4. Subbaiyan, S.; Ponnusamy, I. Biological investigations of ruthenium (III) 3-(Benzothiazol-2-liminomethyl)-phenol Schiff base complexes bearing PPh3/AsPh3 coligand. *Current Chemistry Letters* **2019**, *8*, 145-156, https://doi.org/10.5267/j.ccl.2019.4.003.
5. De, S; Jain, A; Barman, P. Recent Advances in the Catalytic Applications of Chiral Schiff-Base Ligands and Metal Complexes in Asymmetric Organic Transformations. *Chemistry Select*, **2022**, *7*, 1–24, https://doi.org/10.1002/slct.202104334 .
6. Oklu, N.K.; Makhubela, B.C.E. Chemoselective and efficient catalytic hydrogenation of furfural by iridium and ruthenium half-sandwich complexes. *New J. Chem.* **2020**, *44*, 9382-9390, https://doi.org/10.1039/d0nj01811b.
7. Bagra, N; Jain, R. Synthesis of 5-Alkynyl and 2,5-Dialkynyl-L-Histidines. *Chemistry Select* **2022**, 7, 1–4, https://doi.org/10.1002/slct.202200264 .
8. Hooshmand, SE; Jahanpeimay Sabet, M; Hasanzadeh, A; Kamrani Mousavi, SM; Haeri Moghaddam, N; Hooshmand, SA; Rabiee, N; Liu, Y; Hamblin, MR; Karimi, M. Histidine-Enhanced Gene Delivery Systems: The State of the Art. *J Gene Med*, **2022**, 24, 1–31, https://doi.org/10.1002/jgm.3415 .
9. Azza A, S.; Faten, Z.; Aisha, A.T. Synthesis, Characterization, Physicochemical Studies and Antimicrobial Evaluation of Mixed Ligand Complexes Involving Co (II) with 2, 2-Dipyridylamine and Dicarboxylic Acids. *Journal of Transition Metal Complexes* **2020**, *3*, 11, https://doi.org/10.32371/jtmc/246098.
10. Gavisiddegowda, P.; Rajashekhar, D.N.; Kollur, S.P.; Doddarevanna, R.H. Biological Potency of New Benzimidazole Derived Imine Based Ligand and its Co (III), Ni (II), Cu (II) and Pt (II) Complexes: Synthesis, Structure, Antimicrobial, Antioxidant and BSA Interaction Studies. *Bioonterface Res. Appl. Chem.* **2021**, *11*, 11856–11890, https://doi.org/10.33263/BRIAC114.1185611890.

11. Aliabadi, A.; Hakimi, M.; Hosseinabadi, F.; Motieiyan, E.; Rodrigues, V.H.N.; Ghadermazi, M.; Marabello, D.; Abdolmaleki, S. Investigation of X-ray crystal structure and in vitro cytotoxicity of two Ga(III) complexes containing pyridine dicarboxylic acid derivatives and 2-aminobenzimidazole. *J. Mol. Struct.* **2021**, *1223*, 129005, https://doi.org/10.1016/j.molstruc.2020.129005.
12. Pk, EH; Parvin, M; Begum, S; Salam, A. Materials Today : Proceedings Synthesis, Characterization and Biological Activities Study of Metal Complexes of 5 , 6-Dimethylbenzimidazole with Co (II), Cu (II), Cd (II) and Hg (II). *Mater Today Proc*, **2022**, 65, 2743-2751, https://doi.org/10.1016/j.matpr.2022.06.018 .
13. Mustafa, G; Mehmood, R; Mahrosh, HS; Mehmood, K; Ahmed, S. Investigation of Plant Antimicrobial Peptides against Selected Pathogenic Bacterial Species Using a Peptide-Protein Docking Approach. *Biomed Res Int* **2022**, 2022, https://doi.org/10.1155/2022/1077814 .
14. El-Safty, SM; El-Wakiel, N; El-Oleimy, G; Gaber, M; El-Sayed, YS. Microhardness and Fluoride Release of Glass Ionomer Cement Modified with a Novel Al+3Complex to Enhance Its Antimicrobial Activity. *Int J Biomater* .**2021**, 2021, https://doi.org/10.1155/2021/1925388 .
15. El-Sayed, YS; Gaber, M; El-Nahass, MN. Structural Elucidation, Spectroscopic, and Metalochromic Studies of 2-(2-Hydroxy Phenyl)-1-H–Benzimidazole Complexes: Metal Ions Sensing, DNA Binding, and Antimicrobial Activity Evaluation. *J Mol Struct* .**2021**, 1229, 129809, https://doi.org/10.1016/j.molstruc.2020.129809 .
16. Chaudhari, S.R.; Patil, P.N.; Patil, U.K.; Patel, H.M.; Rajput, J.D.; Pawar, N.S.; Patil, D.B. Green synthesis of N-substituted benzimidazoles: The promising methicillin resistant *Staphylococcus aureus* (MRSA) inhibitors. *Chemical Data Collections* **2020**, *25*, 100344, https://doi.org/10.1016/j.cdc.2020.100344.
17. Moreira, NM; dos Santos, JRN; Correa, A. Greener Synthesis of Pyrroloquinazoline Derivatives: Recent Advances. *European J Org Chem*, **2022**, 202200369, https://doi.org/10.1002/ejoc.202200369 .
18. Alminderej, FM; Aroua, LM. Design, Synthesis, Characterization and Anticancer Evaluation of Novel Mixed Complexes Derived from 2-(1H-Benzimizadol-2-Yl)Aniline Schiff Base and 2-Mercaptobenzimidazole or 2-Aminobenzothiazole. *Egypt J Chem* .**2021**, 64, 3351–3364, https://doi.org/10.21608/ejchem.2021.60640.3305.
19. Arunadevi, N; Kanchana, P; Hemapriya, V; Mehala, M; Swathika, M; Chung, IM; Prabakaran, M. A Two-Step Strategy to Synthesis New Aminoguanidinium Complexes: Cytotoxic Effect and Perspectives. *Inorg Nano-Metal Chem* .2022, 0, 1–19, https://doi.org/10.1080/24701556.2022.2081193 .
20. Zayed, EM. New Ligand Metal Complexes: Synthesis, Spectroscopic, DFT, and Docking Studies, and Molecular Structure. *Egypt J Chem*, **2022**, 65, 281–291, https://doi.org/10.21608/EJCHEM.2022.111936.5087 .
21. Shoair, A.F.; El-Bindary, A.A.; El-Ghamaz, N.A.; Rezk, G.N. Synthesis, characterization, DNA binding and antitumor activities of Cu(II) complexes. *J. Mol. Liq.* **2018**, *269*, 619-638, https://doi.org/10.1016/j.molliq.2018.08.075.
22. Sony, A.S.; Suresh, X. Molecular Modeling and Docking Studies of Some Benzodiazole Derivatives on the Protein of *Staphylococcus aureus*. *Journal of Pharmaceutical Research International* **2020**, 102-110, https://doi.org/10.9734/jpri/2020/v32i2930890.
23. Ehrman, J.N.; Lim, V.T.; Bannan, C.C.; Thi, N.; Kyu, D.Y.; Mobley, D.L. Improving small molecule force fields by identifying and characterizing small molecules with inconsistent parameters. *J. Comput.-Aided Mol. Des.* **2021**, *35*, 1-14, https://doi.org/10.26434/chemrxiv.12846602.v1.
24. Li, C.; Sun, J.; Palade, V. Diversity-guided Lamarckian random drift particle swarm optimization for flexible ligand docking. *BMC Bioinformatics*, **2020**, *21*, 286, https://doi.org/10.1186/s12859-020-03630-2.
25. Araújo, J.L.; Bastos, R.S.; Santos, G.T.; de Moraes Alves, M.M.; Figueiredo, K.A.; de Sousa, L.A.; Passos, I.N.G.; de Amorim Carvalho, F.A.; das Chagas Alves Lima, F.; Rocha, J.A. Molecular Docking and Evaluation of Antileishmania Activity of a Ruthenium Complex with Epiisopiloturine and Nitric Oxide. *J. Biosci. Med.* **2020**, *8*, 42–53, https://doi.org/10.4236/jbm.2020.85005.
26. Marinescu, G.; Culita, D.C.; Romanitan, C.; Somacescu, S.; Ene, C.D.; Marinescu, V.; Negreanu, D.G.; Maxim, C.; Popa, M.; Marutescu, L.; Stan, M.; Chifiriuc, C. Novel hybrid materials based on heteroleptic Ru(III) complexes immobilized on SBA-15 mesoporous silica as highly potent antimicrobial and cytotoxic agents. *Appl. Surf. Sci.* **2020**, *520*, 146379, https://doi.org/10.1016/j.apsusc.2020.146379.
27. Bernhard, D.; Schwaiger, W.; Crazzolara, R.; Tinhofer, I.; Kofler, R.; Csordas, A. Enhanced MTT-reducing activity under growth inhibition by resveratrol in CEM-C7H2 lymphocytic leukemia cells. *Cancer Lett.* **2003**, *195*, 193-199, https://doi.org/10.1016/S0304-3835(03)00157-5.
28. Peng, L.; Wang, Y.; Fei, S.; Wei, C.; Tong, F.; Wu, G.; Ma, H.; Dong, X. The effect of combining Endostar with radiotherapy on blood vessels, tumor-associated macrophages, and T cells in brain metastases of Lewis lung cancer. *Translational Lung Cancer Research* **2020**, *9*, 745, https://doi.org/10.21037/tlcr-20-500.

29. El-Gazzar, A.B.A.; Youssef, M.M.; Youssef, A.M.S.; Abu-Hashem, A.A.; Badria, F.A. Design and synthesis of azolopyrimidoquinolines, pyrimidoquinazolines as antioxidant, anti-inflammatory and analgesic activities. *Eur. J. Med. Chem.* **2009**, *44*, 609-624, https://doi.org/10.1016/j.ejmech.2008.03.022.
30. Maurya, M.; Agarwal, N.; Behl, S. Synthesis and characterization of metal complexes of methylene bridged hexadentate tetraanionic ligands. *Indian Journal of Chemistry - Section A Inorganic, Physical, Theoretical and Analytical Chemistry* **2000**, *39*, 1093-1097, https://doi.org/10.4236/ojic.2015.54011 .
31. Kisku, T., Paul, K., Singh, B., Das, S., Mukherjee, S., Kundu, A., Sekhar Das, R. Synthesis of Cu(II)-Caffeine Complex as potential therapeutic Agent: Studies on Antioxidant, anticancer and pharmacological activities. *J. Mol. Liq*., **2022**, 364, 119897, https://doi.org/10.1016/j.molliq.2022.119897.
32. Shoair, A.F.; El-Bindary, A.A.; Abd El-Kader, M.K. Structural and catalytic properties of some azo-rhodanine Ruthenium(III) complexes. *J. Mol. Struct.* **2017**, *1143*, 100-115, https://doi.org/10.1016/j.molstruc.2017.03.109.
33. Fostiak, L.M.; García, I.; Swearingen, J.K.; Bermejo, E.; Castiñeiras, A.; West, D.X. Structural and spectral characterization of transition metal complexes of 2-pyridineformamide N(4)-dimethylthiosemicarbazone. *Polyhedron* **2003**, *22*, 83-92, https://doi.org/10.1016/S0277-5387(02)01330-X.
34. Baird, I.R.; Patrick, B.O.; Skov, K.A.; James, B.R. Ruthenium(III and II) β-diketonate complexes containing imidazoles. *Inorg. Chim. Acta* **2017**, *466*, 565-577, https://doi.org/10.1016/j.ica.2017.07.016.
35. Krishnamoorthy, P.; Sathyadevi, P.; Cowley, A.H.; Butorac, R.R.; Dharmaraj, N. Evaluation of DNA binding, DNA cleavage, protein binding and *in vitro* cytotoxic activities of bivalent transition metal hydrazone complexes. *Eur. J. Med. Chem.* **2011**, *46*, 3376-3387, https://doi.org/10.1016/j.ejmech.2011.05.001.
34. Asmaa Ibrahim , Hanan Elhaes , Medhat Ibrahim , Ibrahim S. Yahia, H.Z. Molecular modeling analyses for polyvinylidene X (X=F, Cl, Br and I). *Biointerface Res. Appl. Chem.* **2020**, *10*, 5556–5563, https://doi.org/10.33263/BRIAC92.890893.
36. Koley, M.K.; Chouhan, O.P.; Biswas, S.; Fernandes, J.; Banerjee, A.; Chattopadhyay, A.; Varghese, B.; Manoharan, P.T.; Koley, A.P. Spectroscopic, electrochemical and DNA binding studies of some monomeric copper(II) complexes containing N2S(thiolate)Cu core and N4S(disulfide)Cu core. *Inorg. Chim. Acta* **2017**, *456*, 179-198, https://doi.org/10.1016/j.ica.2016.10.045.
38. Al-Hazmi, G.A.A.; Abou-Melha, K.S.; Althagafi, I.; El-Metwaly, N.; Shaaban, F.; Abdul Galil, M.S.; El-Bindary, A.A. Synthesis and structural characterization of oxovanadium(IV) complexes of dimedone derivatives. *Appl. Organomet. Chem.* **2020**, *34*, e5672, https://doi.org/10.1002/aoc.5672.
39. El-Deen, I.M.; Shoair, A.F.; El-Bindary, M.A. Synthesis, structural characterization, molecular docking and DNA binding studies of copper complexes. *J. Mol. Liq.* **2018**, *249*, 533-545, https://doi.org/10.1016/j.molliq.2017.11.072.
40. Sumaryada, T.; Astarina, A.S.; Ambarsari, L. Molecular Docking and Physicochemical Analysis of the Active Compounds of Soursop (Annona muricata Linn) for an Anti-Breast Cancer Agent. **2021**, *11*, 11380–11389, https://doi.org/10.33263/BRIAC114.1138011389.
41. Lopes, F.G.; Oliveira, K.A.; Lopes, R.G.; Poluceno, G.G.; Simioni, C.; Da Silva Pescador, G.; Bauer, C.M.; Maraschin, M.; Derner, R.B.; Garcez, R.C. Anti-cancer Effects of Fucoxanthin on Human Glioblastoma Cell Line. *Anticancer Res.* **2020**, *40*, 6799-6815, https://doi.org/10.21873/anticanres.14703.
42. Stura, E.A.; Muller, B.H.; Bossus, M.; Michel, S.; Jolivet-Reynaud, C.; Ducancel, F. Crystal Structure of Human Prostate-Specific Antigen in a Sandwich Antibody Complex. *J. Mol. Biol.* **2011**, *414*, 530-544, https://doi.org/10.1016/j.jmb.2011.10.007 .
43. Beteringhe, A.; Racuciu, C.; Balan, C.; Stoican, E.; Patron, L. Molecular docking studies involving transitional metal complexes (Zn (II), Co (II), Cu (II), Fe (II), Ni (II) with cholic acid (AC) as ligand against Aurora A kinase. **2013**, *787*, 236-240, https://doi.org/10.4028/www.scientific.net/AMR.787.236 .
44. El-Bindary, A.A.; Toson, E.A.; Shoueir, K.R.; Aljohani, H.A.; Abo-Ser, M.M. Metal–organic frameworks as efficient materials for drug delivery: Synthesis, characterization, antioxidant, anticancer, antibacterial and molecular docking investigation. *Appl. Organomet. Chem.* **2020**, *34*, e5905, https://doi.org/10.1002/aoc.5905.
45. Moniruzzaman, M.; Kuddus, M.R.; Chowdhury, A.M.S.; Rashid, M.A. Antioxidant, antimicrobial, anti-diarrheal and analgesic activities of Diospyros malabarica (Desr.) Kostel. *Bangladesh Pharmaceutical Journal* **2019**, *22*, 27-33, https://doi.org/10.3329/bpj.v22i1.40022 .

Supplementary materials

Table S1. The bond lengths and bond angles of complex (1).

Bond lengths (Å)		Bond angles (°)		Bond angles (°)	
		O(13)-H(27)	1.048	N(11)-Ru(12)-Cl(14)	88.695
O(13)-H(27)	1.048	O(13)-H(26)	1.047	O(13)-Ru(12)-Cl(15)	83.908
O(13)-H(26)	1.047	N(11)-H(25)	1.075	O(13)-Ru(12)-Cl(14)	83.711
N(11)-H(25)	1.075	N(11)-H(24)	1.103	Cl(15)-Ru(12)-Cl(14)	167.415
N(11)-H(24)	1.103	C(10)-H(23)	1.116	H(25)-N(11)-H(24)	74.550
C(10)-H(23)	1.116	C(10)-H(22)	1.116	H(25)-N(11)-Ru(12)	112.028
C(10)-H(22)	1.116	N(9)-H(21)	1.045	H(25)-N(11)-C(10)	86.504
N(9)-H(21)	1.045	C(6)-H(20)	1.101	H(24)-N(11)-Ru(12)	105.094
C(6)-H(20)	1.101	C(3)-H(19)	1.102	H(24)-N(11)-C(10)	146.338
C(3)-H(19)	1.102	C(2)-H(18)	1.103	Ru(12)-N(11)-C(10)	107.770
C(2)-H(18)	1.103	C(1)-H(17)	1.103	H(23)-C(10)-H(22)	108.875
C(1)-H(17)	1.103	Ru(12)-Cl(16)	2.246	H(23)-C(10)-N(11)	111.106
Ru(12)-Cl(16)	2.246	N(7)-Ru(12)	1.942	H(23)-C(10)-C(8)	110.976
N(7)-Ru(12)	1.942	N(11)-Ru(12)	1.971	H(22)-C(10)-N(11)	111.624
N(11)-Ru(12)	1.971	O(13)-Ru(12)	1.939	H(22)-C(10)-C(8)	110.710
O(13)-Ru(12)	1.939	Ru(12)-Cl(15)	2.248	N(11)-C(10)-C(8)	103.497
Ru(12)-Cl(15)	2.248	Ru(12)-Cl(14)	2.247	H(21)-N(9)-C(5)	126.048
Ru(12)-Cl(14)	2.247	C(10)-N(11)	1.582	H(21)-N(9)-C(8)	126.537
C(10)-N(11)	1.582	C(8)-C(10)	1.497	C(5)-N(9)-C(8)	107.412
C(8)-C(10)	1.497	N(9)-C(5)	1.265	C(10)-C(8)-N(9)	129.309
N(9)-C(5)	1.265	C(8)-N(9)	1.271	C(10)-C(8)-N(7)	117.843
C(8)-N(9)	1.271	N(7)-C(8)	1.277	N(9)-C(8)-N(7)	112.537
N(7)-C(8)	1.277	C(4)-N(7)	1.273	Ru(12)-N(7)-C(8)	104.053
C(4)-N(7)	1.273	C(6)-C(1)	1.344	Ru(12)-N(7)-C(4)	119.564
C(6)-C(1)	1.344	C(5)-C(6)	1.336	C(8)-N(7)-C(4)	104.271
C(5)-C(6)	1.336	C(4)-C(5)	1.344	H(20)-C(6)-C(1)	121.582
C(4)-C(5)	1.344	C(3)-C(4)	1.343	H(20)-C(6)-C(5)	121.118
C(3)-C(4)	1.343	C(2)-C(3)	1.345	C(1)-C(6)-C(5)	117.278
C(2)-C(3)	1.345	C(1)-C(2)	1.345	N(9)-C(5)-C(6)	130.998
C(1)-C(2)	1.345	H(27)-O(13)-H(26)	159.273	N(9)-C(5)-C(4)	105.796
		H(27)-O(13)-Ru(12)	101.008	C(6)-C(5)-C(4)	123.187

	H(26)-O(13)-Ru(12)	99.686	N(7)-C(4)-C(5)	109.760
	Cl(16)-Ru(12)-N(7)	107.611	N(7)-C(4)-C(3)	131.288
	Cl(16)-Ru(12)-N(11)	167.095	C(5)-C(4)-C(3)	118.732
	Cl(16)-Ru(12)-O(13)	84.749	H(19)-C(3)-C(4)	120.974
	Cl(16)-Ru(12)-Cl(15)	89.895	H(19)-C(3)-C(2)	120.192
	Cl(16)-Ru(12)-Cl(14)	91.209	C(4)-C(3)-C(2)	118.828
	N(7)-Ru(12)-N(11)	85.101	H(18)-C(2)-C(3)	119.368
	N(7)-Ru(12)-O(13)	166.929	H(18)-C(2)-C(1)	119.461
	N(7)-Ru(12)-Cl(15)	91.709	C(3)-C(2)-C(1)	121.168
	N(7)-Ru(12)-Cl(14)	99.893	H(17)-C(1)-C(6)	119.613
	N(11)-Ru(12)-O(13)	82.413	H(17)-C(1)-C(2)	119.816
	N(11)-Ru(12)-Cl(15)	87.447	C(6)-C(1)-C(2)	120.522

Table S2. The bond lengths and bond angles of complex (2).

Bond lengths (Å)		**Bond angles (°)**		**Bond angles (°)**	
C(1)-C(2)	1.838	C(47)-C(48)-C(49)	122.027	C(16)-C(17)-C(18)	119.848
C(2)-C(3)	1.498	C(47)-C(48)-H(90)	127.105	C(16)-C(17)-H(63)	120.794
C(3)-C(4)	1.437	C(49)-C(48)-H(90)	110.763	C(18)-C(17)-H(63)	118.801
C(4)-C(5)	1.420	C(46)-C(47)-C(48)	117.305	C(19)-C(20)-C(15)	116.304
C(5)-C(6)	1.393	C(46)-C(47)-H(89)	122.458	C(19)-C(20)-H(66)	117.714
C(6)-C(1)	1.465	C(48)-C(47)-H(89)	119.174	C(15)-C(20)-H(66)	125.982
C(4)-N(7)	1.258	C(45)-C(46)-C(47)	122.378	C(15)-C(16)-C(17)	118.069
N(7)-C(8)	1.257	C(45)-C(46)-H(88)	110.061	C(15)-C(16)-H(62)	122.587
C(8)-N(9)	1.279	C(47)-C(46)-H(88)	127.560	C(17)-C(16)-H(62)	119.319
N(9)-C(5)	1.280	C(48)-C(49)-C(50)	119.139	As(13)-C(27)-C(28)	101.658
C(8)-C(10)	1.488	C(48)-C(49)-H(91)	116.875	As(13)-C(27)-C(32)	136.538
C(10)-N(11)	1.584	C(50)-C(49)-H(91)	123.695	C(28)-C(27)-C(32)	113.326
As(13)-C(15)	1.976	C(46)-C(45)-C(50)	118.571	As(13)-C(21)-C(22)	126.808
As(13)-C(27)	2.010	C(46)-C(45)-H(87)	121.717	As(13)-C(21)-C(26)	117.278
N(11)-Ru(12)	1.981	C(50)-C(45)-H(87)	119.682	C(22)-C(21)-C(26)	114.700
N(7)-Ru(12)	1.926	C(42)-C(43)-C(44)	118.698	As(13)-C(15)-C(16)	118.956
As(13)-Ru(12)	2.484	C(42)-C(43)-H(85)	121.953	As(13)-C(15)-C(20)	116.979
C(21)-As(13)	1.978	C(44)-C(43)-H(85)	119.346	C(16)-C(15)-C(20)	124.027
C(33)-As(14)	1.972	C(41)-C(42)-C(43)	118.273	C(33)-As(14)-C(39)	103.746

C(39)-As(14)	1.974	C(41)-C(42)-H(84)	126.060	C(33)-As(14)-C(50)	98.756
C(50)-As(14)	1.973	C(43)-C(42)-H(84)	115.666	C(33)-As(14)-Ru(12)	116.800
As(14)-Ru(12)	2.460	C(40)-C(41)-C(42)	124.155	C(39)-As(14)-C(50)	116.381
Cl(51)-Ru(12)	2.250	C(40)-C(41)-H(83)	119.363	C(39)-As(14)-Ru(12)	106.539
Cl(52)-Ru(12)	2.247	C(42)-C(41)-H(83)	116.060	C(50)-As(14)-Ru(12)	114.401
C(15)-C(16)	1.344	C(43)-C(44)-C(39)	121.022	C(15)-As(13)-C(27)	112.552
C(16)-C(17)	1.342	C(43)-C(44)-H(86)	118.276	C(15)-As(13)-Ru(12)	110.813
C(17)-C(18)	1.342	C(39)-C(44)-H(86)	118.661	C(15)-As(13)-C(21)	108.456
C(18)-C(19)	1.342	C(39)-C(40)-C(41)	117.197	C(27)-As(13)-Ru(12)	117.818
C(19)-C(20)	1.342	C(39)-C(40)-H(82)	128.419	C(27)-As(13)-C(21)	92.369
C(15)-C(20)	1.343	C(41)-C(40)-H(82)	114.290	Ru(12)-As(13)-C(21)	113.328
C(21)-C(22)	1.343	C(36)-C(37)-C(38)	118.501	C(10)-N(11)-Ru(12)	115.411
C(22)-C(23)	1.342	C(36)-C(37)-H(80)	122.154	C(10)-N(11)-H(60)	102.044
C(23)-C(24)	1.341	C(38)-C(37)-H(80)	119.295	C(10)-N(11)-H(61)	91.866
C(24)-C(25)	1.341	C(35)-C(36)-C(37)	119.013	Ru(12)-N(11)-H(60)	140.811
C(25)-C(26)	1.342	C(35)-C(36)-H(79)	113.050	Ru(12)-N(11)-H(61)	95.634
C(21)-C(26)	1.345	C(37)-C(36)-H(79)	127.873	H(60)-N(11)-H(61)	71.066
C(27)-C(28)	1.505	C(34)-C(35)-C(36)	120.041	N(11)-Ru(12)-N(7)	72.807
C(28)-C(29)	1.422	C(34)-C(35)-H(78)	118.005	N(11)-Ru(12)-As(13)	120.876
C(29)-C(30)	1.418	C(36)-C(35)-H(78)	121.749	N(11)-Ru(12)-As(14)	70.859
C(30)-C(31)	1.420	C(37)-C(38)-C(33)	124.697	N(11)-Ru(12)-Cl(51)	80.272
C(31)-C(32)	1.498	C(37)-C(38)-H(81)	116.932	N(11)-Ru(12)-Cl(52)	152.488
C(27)-C(32)	1.848	C(33)-C(38)-H(81)	117.973	N(7)-Ru(12)-As(13)	67.614
C(33)-C(34)	1.343	C(33)-C(34)-C(35)	120.663	N(7)-Ru(12)-As(14)	135.971
C(34)-C(35)	1.342	C(33)-C(34)-H(77)	118.624	N(7)-Ru(12)-Cl(51)	87.749
C(35)-C(36)	1.342	C(35)-C(34)-H(77)	120.592	N(7)-Ru(12)-Cl(52)	129.970
C(36)-C(37)	1.341	As(14)-C(50)-C(49)	122.463	As(13)-Ru(12)-As(14)	112.387
C(37)-C(38)	1.341	As(14)-C(50)-C(45)	117.212	As(13)-Ru(12)-Cl(51)	137.402
C(33)-C(38)	1.342	C(49)-C(50)-C(45)	119.242	As(13)-Ru(12)-Cl(52)	85.397
C(39)-C(40)	1.343	As(14)-C(39)-C(40)	122.942	As(14)-Ru(12)-Cl(51)	109.452
C(40)-C(41)	1.342	As(14)-C(39)-C(44)	116.970	As(14)-Ru(12)-Cl(52)	92.611
C(41)-C(42)	1.342	C(40)-C(39)-C(44)	119.365	Cl(51)-Ru(12)-Cl(52)	85.086
C(42)-C(43)	1.341	As(14)-C(33)-C(34)	111.678	C(8)-C(10)-N(11)	104.730

C(43)-C(44)	1.342	As(14)-C(33)-C(38)	131.687	C(8)-C(10)-H(58)	110.418
C(39)-C(44)	1.344	C(34)-C(33)-C(38)	116.448	C(8)-C(10)-H(59)	112.419
C(45)-C(46)	1.342	C(30)-C(31)-C(32)	118.958	N(11)-C(10)-H(58)	114.096
C(46)-C(47)	1.342	C(30)-C(31)-H(75)	120.506	N(11)-C(10)-H(59)	108.054
C(47)-C(48)	1.342	C(32)-C(31)-H(75)	120.334	H(58)-C(10)-H(59)	107.211
C(48)-C(49)	1.342	C(29)-C(30)-C(31)	125.376	N(7)-C(8)-N(9)	114.069
C(49)-C(50)	1.342	C(29)-C(30)-H(74)	114.765	N(7)-C(8)-C(10)	113.274
C(45)-C(50)	1.342	C(31)-C(30)-H(74)	119.452	N(9)-C(8)-C(10)	132.616
C(1)-H(53)	1.143	C(28)-C(29)-C(30)	127.933	C(8)-N(9)-C(5)	105.204
C(2)-H(54)	1.142	C(28)-C(29)-H(73)	110.752	C(8)-N(9)-H(57)	124.066
C(3)-H(55)	1.103	C(30)-C(29)-H(73)	121.126	C(5)-N(9)-H(57)	127.812
C(6)-H(56)	1.104	C(31)-C(32)-C(27)	115.464	C(5)-C(6)-C(1)	118.981
N(9)-H(57)	1.045	C(31)-C(32)-H(76)	106.560	C(5)-C(6)-H(56)	113.121
C(10)-H(58)	1.114	C(27)-C(32)-H(76)	135.375	C(1)-C(6)-H(56)	127.515
C(10)-H(59)	1.115	C(27)-C(28)-C(29)	118.394	C(4)-N(7)-C(8)	104.586
N(11)-H(60)	1.099	C(27)-C(28)-H(72)	127.740	C(4)-N(7)-Ru(12)	121.479
N(11)-H(61)	1.078	C(29)-C(28)-H(72)	113.781	C(8)-N(7)-Ru(12)	133.333
C(16)-H(62)	1.101	C(24)-C(25)-C(26)	120.414	C(4)-C(5)-C(6)	119.732
C(17)-H(63)	1.103	C(24)-C(25)-H(70)	123.533	C(4)-C(5)-N(9)	103.865
C(18)-H(64)	1.103	C(26)-C(25)-H(70)	116.004	C(6)-C(5)-N(9)	136.381
C(19)-H(65)	1.103	C(23)-C(24)-C(25)	119.097	C(3)-C(4)-C(5)	137.949
C(20)-H(66)	1.101	C(23)-C(24)-H(69)	123.963	C(3)-C(4)-N(7)	115.091
C(22)-H(67)	1.094	C(25)-C(24)-H(69)	116.486	C(5)-C(4)-N(7)	101.568
C(23)-H(68)	1.103	C(22)-C(23)-C(24)	118.634	C(2)-C(3)-C(4)	114.254
C(24)-H(69)	1.103	C(22)-C(23)-H(68)	127.124	C(2)-C(3)-H(55)	101.312
C(25)-H(70)	1.103	C(24)-C(23)-H(68)	114.151	C(4)-C(3)-H(55)	144.255
C(26)-H(71)	1.101	C(25)-C(26)-C(21)	122.514	C(1)-C(2)-C(3)	108.434
C(28)-H(72)	1.101	C(25)-C(26)-H(71)	117.049	C(1)-C(2)-H(54)	137.196
C(29)-H(73)	1.105	C(21)-C(26)-H(71)	120.347	C(3)-C(2)-H(54)	114.091
C(30)-H(74)	1.105	C(21)-C(22)-C(23)	123.579	C(2)-C(1)-C(6)	119.357
C(31)-H(75)	1.105	C(21)-C(22)-H(67)	123.176	C(2)-C(1)-H(53)	131.129
C(32)-H(76)	1.148	C(23)-C(22)-H(67)	113.112	C(6)-C(1)-H(53)	109.460
C(34)-H(77)	1.100	C(18)-C(19)-C(20)	121.212		

C(35)-H(78)	1.103	C(18)-C(19)-H(65)	113.810		
C(36)-H(79)	1.103	C(20)-C(19)-H(65)	124.796		
C(37)-H(80)	1.102	C(17)-C(18)-C(19)	119.838		
C(38)-H(81)	1.098	C(17)-C(18)-H(64)	120.854		
C(40)-H(82)	1.100	C(19)-C(18)-H(64)	119.244		
C(41)-H(83)	1.103				
C(42)-H(84)	1.103				
C(43)-H(85)	1.103				
C(44)-H(86)	1.102				
C(45)-H(87)	1.101				
C(46)-H(88)	1.103				
C(47)-H(89)	1.103				
C(48)-H(90)	1.103				
C(49)-H(91)	1.056				

Table S3. The bond lengths and bond angles of complex (3).

Bond lengths (Å)		**Bond angles (°)**		**Bond angles (°)**	
C(50)-H(91)	1.096	H(91)-C(50)-C(45)	116.106	C(19)-C(18)-C(17)	119.282
C(48)-H(90)	1.102	H(91)-C(50)-C(49)	122.036	H(63)-C(17)-C(18)	119.743
C(47)-H(89)	1.103	C(45)-C(50)-C(49)	121.858	H(63)-C(17)-C(16)	120.061
C(46)-H(88)	1.102	C(50)-C(49)-C(48)	116.756	C(18)-C(17)-C(16)	120.189
C(45)-H(87)	1.103	C(50)-C(49)-P(14)	126.000	H(62)-C(16)-C(17)	117.235
C(44)-H(86)	1.103	C(48)-C(49)-P(14)	117.206	H(62)-C(16)-C(15)	121.398
C(43)-H(85)	1.102	H(90)-C(48)-C(49)	121.185	C(17)-C(16)-C(15)	121.361
C(41)-H(84)	1.101	H(90)-C(48)-C(47)	116.784	C(20)-C(15)-C(16)	117.535
C(40)-H(83)	1.103	C(49)-C(48)-C(47)	122.031	C(20)-C(15)-P(13)	120.128
C(39)-H(82)	1.103	H(89)-C(47)-C(48)	120.153	C(16)-C(15)-P(13)	122.207
C(38)-H(81)	1.103	H(89)-C(47)-C(46)	119.801	C(36)-P(14)-C(42)	107.489
C(37)-H(80)	1.101	C(48)-C(47)-C(46)	120.046	C(36)-P(14)-C(49)	101.376
C(35)-H(79)	1.096	H(88)-C(46)-C(47)	120.481	C(36)-P(14)-Ru(12)	116.911
C(34)-H(78)	1.103	H(88)-C(46)-C(45)	120.497	C(42)-P(14)-C(49)	102.625
C(33)-H(77)	1.102	C(47)-C(46)-C(45)	119.019	C(42)-P(14)-Ru(12)	108.779
C(32)-H(76)	1.099	H(87)-C(45)-C(50)	120.096	C(49)-P(14)-Ru(12)	118.309
C(30)-H(75)	1.101	H(87)-C(45)-C(46)	119.636	Ru(12)-P(13)-C(31)	115.161

C(29)-H(74)	1.103	C(50)-C(45)-C(46)	120.267	Ru(12)-P(13)-C(26)	110.012
C(28)-H(73)	1.103	H(86)-C(44)-C(39)	119.909	Ru(12)-P(13)-C(15)	111.118
C(27)-H(72)	1.103	H(86)-C(44)-C(43)	120.004	C(31)-P(13)-C(26)	105.313
C(25)-H(71)	1.100	C(39)-C(44)-C(43)	120.087	C(31)-P(13)-C(15)	103.926
C(24)-H(70)	1.103	H(85)-C(43)-C(44)	118.347	C(26)-P(13)-C(15)	111.056
C(23)-H(69)	1.103	H(85)-C(43)-C(42)	120.834	Cl(52)-Ru(12)-Cl(51)	91.424
C(22)-H(68)	1.103	C(44)-C(43)-C(42)	120.816	Cl(52)-Ru(12)-P(13)	83.553
C(21)-H(67)	1.099	C(43)-C(42)-C(41)	118.536	Cl(52)-Ru(12)-P(14)	87.312
C(20)-H(66)	1.102	C(43)-C(42)-P(14)	119.747	Cl(52)-Ru(12)-N(11)	91.864
C(19)-H(65)	1.103	C(41)-C(42)-P(14)	121.716	Cl(52)-Ru(12)-N(7)	166.988
C(18)-H(64)	1.103	H(84)-C(41)-C(42)	120.937	Cl(51)-Ru(12)-P(13)	97.927
C(17)-H(63)	1.103	H(84)-C(41)-C(40)	118.183	Cl(51)-Ru(12)-P(14)	87.742
C(16)-H(62)	1.099	C(42)-C(41)-C(40)	120.879	Cl(51)-Ru(12)-N(11)	173.454
N(11)-H(61)	1.101	H(83)-C(40)-C(41)	120.033	Cl(51)-Ru(12)-N(7)	94.907
N(11)-H(60)	1.076	H(83)-C(40)-C(39)	119.930	P(13)-Ru(12)-P(14)	169.347
C(10)-H(59)	1.115	C(41)-C(40)-C(39)	120.037	P(13)-Ru(12)-N(11)	88.068
C(10)-H(58)	1.116	H(82)-C(39)-C(44)	120.175	P(13)-Ru(12)-N(7)	84.321
N(9)-H(57)	1.045	H(82)-C(39)-C(40)	120.191	P(14)-Ru(12)-N(11)	86.760
C(6)-H(56)	1.101	C(44)-C(39)-C(40)	119.629	P(14)-Ru(12)-N(7)	104.261
C(3)-H(55)	1.102	H(81)-C(38)-C(33)	119.786	N(11)-Ru(12)-N(7)	83.020
C(2)-H(54)	1.103	H(81)-C(38)-C(37)	120.151	H(61)-N(11)-H(60)	73.609
C(1)-H(53)	1.103	C(33)-C(38)-C(37)	120.060	H(61)-N(11)-Ru(12)	104.901
C(45)-C(50)	1.343	H(80)-C(37)-C(38)	116.734	H(61)-N(11)-C(10)	143.731
C(49)-C(50)	1.345	H(80)-C(37)-C(36)	121.226	H(60)-N(11)-Ru(12)	111.301
C(48)-C(49)	1.348	C(38)-C(37)-C(36)	122.040	H(60)-N(11)-C(10)	85.543
C(47)-C(48)	1.342	C(37)-C(36)-C(35)	116.688	Ru(12)-N(11)-C(10)	110.288
C(46)-C(47)	1.340	C(37)-C(36)-P(14)	118.513	H(59)-C(10)-H(58)	108.288
C(45)-C(46)	1.340	C(35)-C(36)-P(14)	124.685	H(59)-C(10)-N(11)	111.438
C(39)-C(44)	1.341	H(79)-C(35)-C(36)	122.179	H(59)-C(10)-C(8)	111.261
C(43)-C(44)	1.342	H(79)-C(35)-C(34)	115.933	H(58)-C(10)-N(11)	111.487
C(42)-C(43)	1.346	C(36)-C(35)-C(34)	121.885	H(58)-C(10)-C(8)	110.283
C(41)-C(42)	1.345	H(78)-C(34)-C(35)	120.114	N(11)-C(10)-C(8)	104.081
C(40)-C(41)	1.342	H(78)-C(34)-C(33)	119.637	H(57)-N(9)-C(5)	125.969

C(39)-C(40)	1.341	C(35)-C(34)-C(33)	120.243	H(57)-N(9)-C(8)	126.598
C(33)-C(38)	1.340	H(77)-C(33)-C(38)	120.489	C(5)-N(9)-C(8)	107.428
C(37)-C(38)	1.342	H(77)-C(33)-C(34)	120.501	C(10)-C(8)-N(9)	128.773
C(36)-C(37)	1.348	C(38)-C(33)-C(34)	118.996	C(10)-C(8)-N(7)	118.262
C(35)-C(36)	1.346	H(76)-C(32)-C(27)	117.033	N(9)-C(8)-N(7)	112.922
C(34)-C(35)	1.342	H(76)-C(32)-C(31)	121.371	Ru(12)-N(7)-C(8)	108.932
C(33)-C(34)	1.340	C(27)-C(32)-C(31)	121.595	Ru(12)-N(7)-C(4)	125.755
C(27)-C(32)	1.342	C(32)-C(31)-C(30)	117.366	C(8)-N(7)-C(4)	103.857
C(31)-C(32)	1.346	C(32)-C(31)-P(13)	123.172	H(56)-C(6)-C(1)	121.421
C(30)-C(31)	1.347	C(30)-C(31)-P(13)	119.416	H(56)-C(6)-C(5)	121.179
C(29)-C(30)	1.342	H(75)-C(30)-C(31)	121.371	C(1)-C(6)-C(5)	117.374
C(28)-C(29)	1.340	H(75)-C(30)-C(29)	117.118	N(9)-C(5)-C(6)	130.325
C(27)-C(28)	1.340	C(31)-C(30)-C(29)	121.511	N(9)-C(5)-C(4)	105.672
C(21)-C(26)	1.346	H(74)-C(29)-C(30)	120.080	C(6)-C(5)-C(4)	123.968
C(25)-C(26)	1.346	H(74)-C(29)-C(28)	119.754	N(7)-C(4)-C(5)	110.033
C(24)-C(25)	1.342	C(30)-C(29)-C(28)	120.165	N(7)-C(4)-C(3)	132.054
C(23)-C(24)	1.340	H(73)-C(28)-C(29)	120.390	C(5)-C(4)-C(3)	117.335
C(22)-C(23)	1.340	H(73)-C(28)-C(27)	120.377	H(55)-C(3)-C(4)	121.331
C(21)-C(22)	1.342	C(29)-C(28)-C(27)	119.227	H(55)-C(3)-C(2)	119.027
C(15)-C(20)	1.347	H(72)-C(27)-C(32)	120.084	C(4)-C(3)-C(2)	119.642
C(19)-C(20)	1.342	H(72)-C(27)-C(28)	119.811	H(54)-C(2)-C(3)	119.433
C(18)-C(19)	1.340	C(32)-C(27)-C(28)	120.102	H(54)-C(2)-C(1)	119.413
C(17)-C(18)	1.341	C(21)-C(26)-C(25)	117.307	C(3)-C(2)-C(1)	121.133
C(16)-C(17)	1.342	C(21)-C(26)-P(13)	120.450	H(53)-C(1)-C(6)	119.798
C(15)-C(16)	1.345	C(25)-C(26)-P(13)	122.229	H(53)-C(1)-C(2)	120.045
Cl(52)-Ru(12)	2.250	H(71)-C(25)-C(26)	120.998	C(6)-C(1)-C(2)	120.058
Cl(51)-Ru(12)	2.248	H(71)-C(25)-C(24)	117.283		
P(13)-Ru(12)	2.365	C(26)-C(25)-C(24)	121.717		
P(13)-C(31)	1.880	H(70)-C(24)-C(25)	120.079		
P(13)-C(26)	1.874	H(70)-C(24)-C(23)	119.897		
C(15)-P(13)	1.871	C(25)-C(24)-C(23)	120.023		
C(36)-P(14)	1.880	H(69)-C(23)-C(24)	120.370		
P(14)-C(42)	1.873	H(69)-C(23)-C(22)	120.398		

C(49)-P(14)	1.887	C(24)-C(23)-C(22)	119.231		
P(14)-Ru(12)	2.362	H(68)-C(22)-C(23)	119.753		
N(11)-Ru(12)	1.972	H(68)-C(22)-C(21)	120.064		
N(7)-Ru(12)	1.947	C(23)-C(22)-C(21)	120.183		
C(10)-N(11)	1.574	H(67)-C(21)-C(26)	121.343		
C(8)-C(10)	1.493	H(67)-C(21)-C(22)	117.118		
N(9)-C(5)	1.263	C(26)-C(21)-C(22)	121.538		
C(8)-N(9)	1.269	H(66)-C(20)-C(15)	120.949		
N(7)-C(8)	1.276	H(66)-C(20)-C(19)	117.543		
C(4)-N(7)	1.275	C(15)-C(20)-C(19)	121.504		
C(6)-C(1)	1.342	H(65)-C(19)-C(20)	120.081		
C(5)-C(6)	1.336	H(65)-C(19)-C(18)	119.888		
C(4)-C(5)	1.343	C(20)-C(19)-C(18)	120.026		
C(3)-C(4)	1.345	H(64)-C(18)-C(19)	120.338		
C(2)-C(3)	1.344	H(64)-C(18)-C(17)	120.361		
C(1)-C(2)	1.344				

Table S4. The bond lengths and bond angles of complex (4).

Bond lengths (Å)		**Bond angles (º)**		**Bond angles (º)**	
C(36)-H(61)	1.103	H(61)-C(36)-N(31)	119.072	C(15)-C(14)-C(13)	125.017
C(35)-H(60)	1.102	H(61)-C(36)-C(35)	110.486	H(46)-C(13)-C(18)	76.250
C(34)-H(59)	1.102	N(31)-C(36)-C(35)	129.920	H(46)-C(13)-C(14)	75.413
C(33)-H(58)	1.101	H(60)-C(35)-C(36)	127.056	C(18)-C(13)-C(14)	89.602
C(28)-H(57)	1.100	H(60)-C(35)-C(34)	127.043	N(31)-Ru(12)-N(30)	78.074
C(27)-H(56)	1.102	C(36)-C(35)-C(34)	105.848	N(31)-Ru(12)-N(23)	82.413
C(26)-H(55)	1.102	H(59)-C(34)-C(35)	121.229	N(31)-Ru(12)-N(17)	114.546
C(25)-H(54)	1.100	H(59)-C(34)-C(33)	124.171	N(31)-Ru(12)-N(11)	87.869
C(22)-H(53)	1.111	C(35)-C(34)-C(33)	114.572	N(31)-Ru(12)-N(7)	163.110
C(21)-H(52)	1.098	H(58)-C(33)-C(34)	109.293	N(30)-Ru(12)-N(23)	101.833
C(20)-H(51)	1.102	H(58)-C(33)-C(32)	108.090	N(30)-Ru(12)-N(17)	166.206
C(19)-H(50)	1.111	C(34)-C(33)-C(32)	142.600	N(30)-Ru(12)-N(11)	81.424
C(18)-H(49)	1.105	C(29)-C(32)-C(33)	167.746	N(30)-Ru(12)-N(7)	88.411

C(15)-H(48)	1.111	C(29)-C(32)-N(31)	78.085	N(23)-Ru(12)-N(17)	75.541
C(14)-H(47)	1.102	C(33)-C(32)-N(31)	93.977	N(23)-Ru(12)-N(11)	168.818
C(13)-H(46)	1.098	Ru(12)-N(31)-C(36)	113.559	N(23)-Ru(12)-N(7)	110.570
N(11)-H(45)	1.076	Ru(12)-N(31)-C(32)	100.860	N(17)-Ru(12)-N(11)	103.790
N(11)-H(44)	1.104	C(36)-N(31)-C(32)	130.560	N(17)-Ru(12)-N(7)	80.066
C(10)-H(43)	1.116	Ru(12)-N(30)-C(25)	125.631	N(11)-Ru(12)-N(7)	80.056
C(10)-H(42)	1.115	Ru(12)-N(30)-C(29)	97.086	H(45)-N(11)-H(44)	74.097
N(9)-H(41)	1.045	C(25)-N(30)-C(29)	117.395	H(45)-N(11)-Ru(12)	110.040
C(6)-H(40)	1.101	C(32)-C(29)-N(30)	115.634	H(45)-N(11)-C(10)	86.049
C(3)-H(39)	1.098	C(32)-C(29)-C(28)	120.833	H(44)-N(11)-Ru(12)	101.728
C(2)-H(38)	1.103	N(30)-C(29)-C(28)	123.486	H(44)-N(11)-C(10)	145.430
C(1)-H(37)	1.103	H(57)-C(28)-C(29)	120.567	Ru(12)-N(11)-C(10)	111.682
C(29)-C(32)	1.343	H(57)-C(28)-C(27)	120.661	H(43)-C(10)-H(42)	104.987
C(16)-C(24)	1.367	C(29)-C(28)-C(27)	118.772	H(43)-C(10)-N(11)	117.810
N(31)-Ru(12)	1.951	H(56)-C(27)-C(28)	120.730	H(43)-C(10)-C(8)	113.825
N(30)-Ru(12)	1.948	H(56)-C(27)-C(26)	121.323	H(42)-C(10)-N(11)	110.251
N(23)-Ru(12)	1.965	C(28)-C(27)-C(26)	117.923	H(42)-C(10)-C(8)	111.114
N(17)-Ru(12)	1.964	H(55)-C(26)-C(27)	120.064	N(11)-C(10)-C(8)	98.947
C(36)-N(31)	1.273	H(55)-C(26)-C(25)	120.869	H(41)-N(9)-C(5)	126.597
C(35)-C(36)	1.342	C(27)-C(26)-C(25)	118.685	H(41)-N(9)-C(8)	128.804
C(34)-C(35)	1.338	H(54)-C(25)-N(30)	118.213	C(5)-N(9)-C(8)	103.888
C(33)-C(34)	1.340	H(54)-C(25)-C(26)	117.337	C(10)-C(8)-N(9)	115.197
C(32)-C(33)	1.348	N(30)-C(25)-C(26)	123.584	C(10)-C(8)-N(7)	120.103
N(31)-C(32)	1.278	C(16)-C(24)-C(19)	164.332	N(9)-C(8)-N(7)	117.994
N(30)-C(25)	1.273	C(16)-C(24)-N(23)	78.827	Ru(12)-N(7)-C(8)	110.990
C(29)-N(30)	1.270	C(19)-C(24)-N(23)	89.025	Ru(12)-N(7)-C(4)	130.958
C(28)-C(29)	1.349	Ru(12)-N(23)-C(24)	90.411	C(8)-N(7)-C(4)	98.811
C(27)-C(28)	1.343	Ru(12)-N(23)-C(22)	117.264	H(40)-C(6)-C(1)	121.597
C(26)-C(27)	1.342	C(24)-N(23)-C(22)	133.026	H(40)-C(6)-C(5)	121.330
C(25)-C(26)	1.346	H(53)-C(22)-N(23)	116.907	C(1)-C(6)-C(5)	117.051
C(24)-C(19)	1.360	H(53)-C(22)-C(21)	107.566	N(9)-C(5)-C(6)	125.597
N(23)-C(24)	1.339	N(23)-C(22)-C(21)	135.000	N(9)-C(5)-C(4)	105.111
C(22)-N(23)	1.280	H(52)-C(21)-C(22)	75.744	C(6)-C(5)-C(4)	129.221

C(21)-C(22)	1.332	H(52)-C(21)-C(20)	74.906	N(7)-C(4)-C(5)	114.173
C(20)-C(21)	1.325	C(22)-C(21)-C(20)	90.943	N(7)-C(4)-C(3)	135.735
C(19)-C(20)	1.340	H(51)-C(20)-C(21)	116.488	C(5)-C(4)-C(3)	110.038
C(18)-C(13)	1.331	H(51)-C(20)-C(19)	118.482	H(39)-C(3)-C(4)	124.447
N(17)-C(18)	1.279	C(21)-C(20)-C(19)	124.807	H(39)-C(3)-C(2)	111.020
C(16)-N(17)	1.335	H(50)-C(19)-C(24)	114.852	C(4)-C(3)-C(2)	124.367
C(15)-C(16)	1.363	H(50)-C(19)-C(20)	107.418	H(38)-C(2)-C(3)	119.692
C(14)-C(15)	1.340	C(24)-C(19)-C(20)	137.728	H(38)-C(2)-C(1)	118.567
C(13)-C(14)	1.323	H(49)-C(18)-C(13)	106.475	C(3)-C(2)-C(1)	121.713
N(11)-Ru(12)	1.976	H(49)-C(18)-N(17)	120.596	H(37)-C(1)-C(6)	121.323
N(7)-Ru(12)	1.955	C(13)-C(18)-N(17)	132.914	H(37)-C(1)-C(2)	121.437
C(10)-N(11)	1.568	Ru(12)-N(17)-C(18)	115.617	C(6)-C(1)-C(2)	117.239
C(8)-C(10)	1.488	Ru(12)-N(17)-C(16)	95.693		
N(9)-C(5)	1.262	C(18)-N(17)-C(16)	133.874		
C(8)-N(9)	1.269	C(24)-C(16)-N(17)	80.885		
N(7)-C(8)	1.278	C(24)-C(16)-C(15)	166.466		
C(4)-N(7)	1.276	N(17)-C(16)-C(15)	88.501		
C(6)-C(1)	1.342	H(48)-C(15)-C(16)	111.346		
C(5)-C(6)	1.336	H(48)-C(15)-C(14)	111.663		
C(4)-C(5)	1.344	C(16)-C(15)-C(14)	136.936		
C(3)-C(4)	1.343	H(47)-C(14)-C(15)	118.424		
C(2)-C(3)	1.345	H(47)-C(14)-C(13)	116.286		
C(1)-C(2)	1.344				